

ELECTRO-ABSORPTION MODULATOR IN LITHIUM NIOBATE

A Thesis

by

JAVED ALI

Submitted to the Office of Graduate and Professional Studies of
Texas A&M University
in partial fulfillment of the requirements for the degree of

MASTER OF SCIENCE

Chair of Committee, Ohannes Eknoyan
Committee Members, Philip Hemmer
Alexey Belyanin
Gwan Choi

Head of Department, Miroslav Begovic

August 2017

Major Subject: Electrical Engineering

Copyright 2017 Javed Ali

ABSTRACT

Lithium niobate presents a good choice for integrated optics in optical communications and networks applications. Titanium diffused waveguides in lithium niobate are low loss and have a high coupling efficiency with single mode optical fibers at $1.55\mu\text{m}$ wavelength.

Lithium niobate has also been extensively used to fabricate modulators owing to its high electro-optic coefficients. The modulators fabricated in lithium niobate suffer primarily from large device footprint which makes it difficult to integrate variety of devices on a single chip.

To help overcome this limitation, two device design configurations for electro-absorption modulation is studied. The first architecture consists of a stack of Indium Tin Oxide (ITO)/ SiO_2 /Au films on the lithium niobate waveguide. The second device configuration also consists of ITO/ SiO_2 /Au stack but includes an additional extended TiO_2 film over the waveguide. TiO_2 film having a refractive index higher than lithium niobate shifts the optical field towards the surface of the waveguide. This helps to enhance light matter interaction with ITO which serves as the active material.

Simulation of the device architecture predicts 5.24dB extinction ratio for the first configuration on a $100\mu\text{m}$ device length, and 3.75dB extinction ratio for the second architecture with a $20\mu\text{m}$ modulator length. These are highest reported extinction ratio in lithium niobate based modulators for such a small device footprint.

To my family

ACKNOWLEDGEMENTS

I am thankful to Dr. Ohannes Eknoyan for his guidance and support throughout my stay at Texas A&M University. I would like to thank Dr. Philip Hemmer for his continuous support and guidance for his invaluable discussions and allowing me to use his laboratory for experiments. I am also thankful to Dr. Alexey Belyanin and Dr. Gwan Choi for taking time out of their schedule for their guidance.

I would express my gratitude to Fahad Alghannam, Abdurrahman Almethen and Masfer Al-Kahtani for their support and invaluable suggestions.

Finally, I would like to thank my parents and brother for being constant a source of support and ensuring my well-being. I would like to recognize Naeema Abdusalam for encouraging and motivating me, when I needed it the most.

CONTRIBUTORS AND FUNDING SOURCES

Contributors

This work was supported by a thesis committee consisting of Professor Ohannes Eknoyan, Professor Philip Hemmer and Dr. Gwan Choi of the Department of Electrical and Computer Engineering and Professor Alexey Belyanin of the Department of Physics. All the work conducted for the thesis was completed by the student independently.

Funding Sources

There are no outside funding contributions to acknowledge related to the research and compilation of this document.

TABLE OF CONTENTS

	Page
ABSTRACT.....	ii
DEDICATION.....	iii
ACKNOWLEDGEMENTS.....	iv
CONTRIBUTORS AND FUNDING SOURCES.....	v
TABLE OF CONTENTS.....	vi
LIST OF FIGURES.....	viii
LIST OF TABLES.....	x
CHAPTER I INTRODUCTION.....	1
1.1 Motivation.....	1
1.2 Lithium Niobate Modulators.....	2
1.3 Plasmonic Modulators.....	4
1.4 Organization of the Thesis.....	8
CHAPTER II THEORETICAL BACKGROUND.....	9

2.1 Modal Analysis.....	9
2.2 Dielectric Slab Waveguide.....	11
2.3 Planar Graded Index Waveguide.....	15
2.4 Rectangular Waveguide.....	17
CHAPTER III DEVICE ARCHITECTURE AND SIMULATION.....	24
3.1 Diffused Channel Waveguide Modeling.....	24
3.2 Proposed Modulator Architecture.....	31
3.3 Optical Properties of Indium Tin Oxide (ITO).....	35
3.4 Coupling to TiO ₂	39
3.5 Results and Discussion.....	41
CHAPTER IV CONCLUSION.....	48
REFERENCES.....	50

LIST OF FIGURES

FIGURE	Page
1.1 MZI based electro optic modulator.....	3
1.2 Modulator configuration reported by A.P. Vasudev et al. [4].....	5
1.3 Modulator proposed by Melikyan et al. [5] (a) MIM configuration (b) Proof of principle configuration.....	6
1.4 Modulator integrated with SOI waveguide proposed by Sorger group [2].....	7
2.1 Dielectric slab waveguide structure.....	11
2.2 Eigen value equation graphical plot.....	13
2.3 Field distribution of first two TE modes in a slab waveguide.....	14
2.4 Graded index planar waveguide.....	15
2.5 Rectangular waveguides configuration (a) Rib waveguide (b) Ridge waveguide (c) Diffused channel waveguide (d) Buried waveguide.....	18
2.6 Rectangular waveguide cross section.....	19
2.7 Mode field profiles in rectangular waveguide for (a) E_{00}^x mode (b) E_{10}^x mode (c) E_{00}^y mode (d) E_{10}^y mode.....	23
3.1 Ti diffused channel waveguide in lithium niobate substrate.....	26
3.2 Cross sectional view of Ti diffused channel waveguide with titanium film.....	28

3.3	Refractive index change due to Ti diffusion (a) along depth (b) along lateral direction (c) 2-D profile.....	29
3.4	Architecture 1: Modulator configuration integrated with Ti diffused waveguide.....	33
3.5	Architecture 2 modulator configuration: (a) Perspective view (b) Cross sectional view.....	34
3.6	Optical properties of ITO as a function of wavelength (a) Permittivity real part (b) Permittivity imaginary part(c) Refractive index real part (d) Refractive index imaginary part	36
3.7	ITO refractive index vs. carriers concentration.....	38
3.8	Cross section of the hybrid TiO ₂ and Ti diffused waveguide.....	39
3.9	Electric field distribution for LN waveguide-TiO ₂ hybrid waveguide (a) with position (b) at LN waveguide surface.....	40
3.10	Fundamental TM mode of Ti diffused waveguide.....	41
3.11	Charge carriers concentration corresponding to the ON and the OFF states for Architecture 1 and Architecture 2.....	42
3.12	Field profile for Modulator Architecture 1 (a) OFF state (b) ON state...	44
3.13	Field profile for Modulator Architecture 2 (a) OFF state (b) ON state...	45

LIST OF TABLES

TABLE		Page
1	Performance of various reported modulator architectures.....	8
2	Performance comparison between Architecture 1 and Architecture 2.....	47

CHAPTER I

INTRODUCTION

1.1 Motivation

The ever increasing demand for higher rate data transmission has made photonics one of the foremost choices. The inherent capability of light to support terahertz regime bandwidths is a highly desirable characteristic. A communications system basically has three main components namely transmitter, signal processing unit and a receiver. In case of optical communication system a coherent light source such as a laser typically acts as a transmitter, and a photo-detector acts as a receiver. Signal processing units can have variety of functions like modulation, wavelength selection etc. Digital transmission requires conversion of data from analog domain to digital domain which in turn requires a modulation mechanism.

Varieties of device architecture have been proposed in literature and are commercially available which can modulate an incoming light signal both in phase and intensity. Most of the commercially available devices have a very large footprint which limits the integration density of devices on a single chip. Thus, in order to enhance the functionality of photonic integrated circuits there is a need to integrate more and more devices on a single chip. This can only be accomplished if the size of each device can be

reduced significantly. Currently, only few integrated optical devices can be integrated on a single chip and thus restricting optical signal processing capabilities.

1.2 Lithium Niobate Modulators

Lithium niobate modulators have provided an excellent means for external modulation mechanism. One of the main advantages is that lithium niobate technology is well established and provides stable operation over a wide temperature range. Moreover lithium niobate based devices have a very efficient coupling with optical fibers which makes it a suitable technology for optical communications [1]. Most modulators in lithium niobate can be classified as

- 1) Mach-Zender Interferometer (MZI) type.
- 2) Directional Coupler kind.

In case of MZI type devices, an incident optical signal is split into two arms and then combined back as shown in Fig. 1.1. Electro-optic property of lithium niobate allows modifying the phase of optical signal in each arm by applying electric field across it.

Lithium niobate modulators are commercially available in packaged forms, both as intensity modulators and phase modulators. The performance of these modulators has been optimized for telecommunications wavelength. They are typically available with 10GHz 3dB bandwidth and optical loss of the order of 3-4dB. The RF drive voltage for these modulators is typically in the range of 4-6V.

Although, performance of modulators in lithium niobate is good but the device footprint is too large to integrate multiple devices on a single chip. Electro-optic properties of

lithium niobate makes it one of the best choices to fabricate integrated optical circuits. Lithium niobate is a preferred material because many other active and passive devices can be fabricated on lithium niobate. Phase modulators, polarization converters, intensity modulators, couplers etc. have all been demonstrated on lithium niobate.

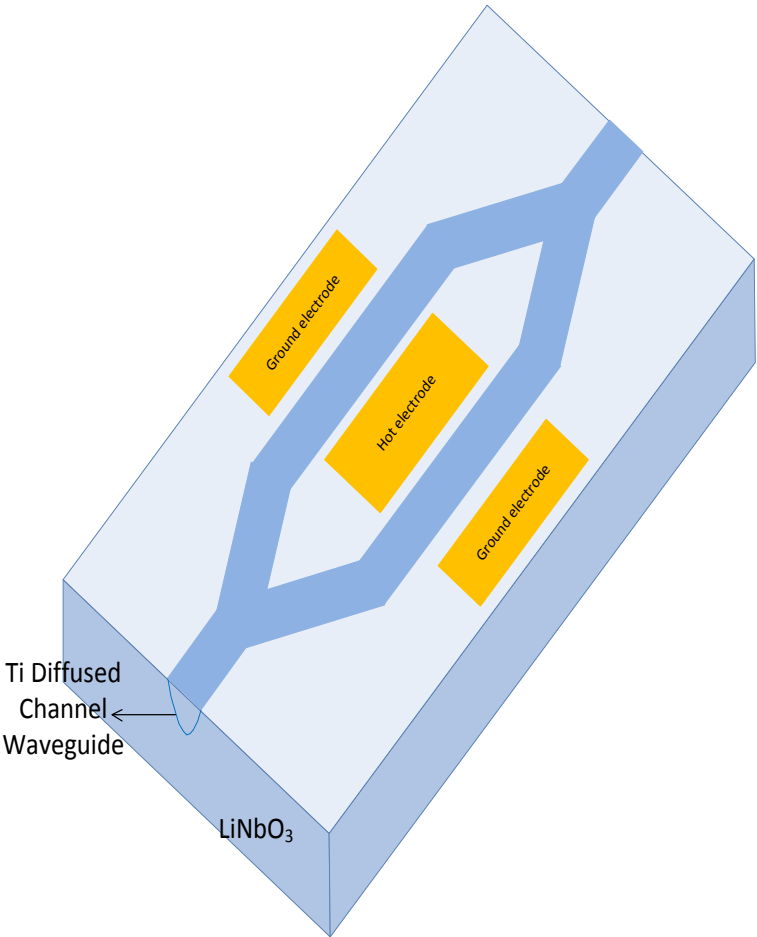


Fig.1.1. MZI based electro optic modulator.

1.3 Plasmonic Modulators

Recent advances have seen a rising interest in plasmonic modulators. Plasmonics can fill the gap between the size of modern day electronics and photonics as surface plasmon polaritons are very tightly confined. They also enable to overcome diffraction limit and thus, it's a way forward for developing a new generation of nano-scale devices with ultrafast response time.

As modulators form one of the very basic components in active optical circuitry, it becomes paramount to explore the architecture of these devices. Indium tin oxide (ITO) has recently emerged as a potential candidate to be used in electro-optic modulators. The refractive index of ITO can be tuned by applying electric field across it. The applied electric field induces accumulation of free charge carriers which in turn is responsible for the change in refractive index. Recent study has shown that the refractive index can be changed substantially [2]. Highly tunable refractive index offers the possibility of using ITO as an active material in optical phase and intensity modulators.

ITO permittivity can be tuned in such a way that the real part of the permittivity approaches zero. This state has been called epsilon near zero (ENZ). Experimental results have shown that modulation is very effective around ENZ regime. Apart from ITO, other materials such as Aluminum zinc oxide (AZO) also exhibit tunability of refractive index with applied voltage bias.

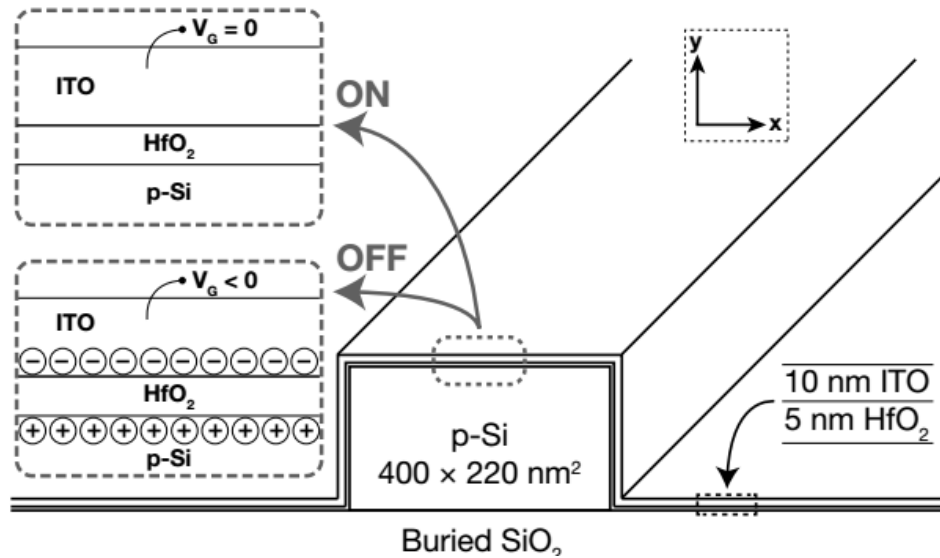


Fig. 1.2 Modulator configuration reported by A.P. Vasudev et al. [4] Reprinted by permission from “Electro-optical modulation of a silicon waveguide with an “epsilon near-zero” material,” by A. P. Vasudev, J. Kang, J. Park, X. Liu & M.L. Brongersma, 2013, Optics Express 21, 26387–26397., Copyright 2013 by Optical Society of America.

Recently, few research groups have reported plasmonic based modulators but very few have experimentally demonstrated actual device operation. Moreover, most of the devices are on silicon substrate. Plasmonic modulators are predominantly of two types of architectures. One of the architectures is based on metal-oxide-semiconductor (MOS) stack, which is a hybrid plasmonic-photonic architecture. The second type is metal-insulator-metal (MIM) structure. The MOS type devices are easy to fabricate and integrate with silicon ridge waveguides. Their size is also comparable to silicon waveguide and thus insertion loss is relatively low. Whereas, in MIM type of design insertion loss is very high as coupling from photonic mode to a plasmonic mode is very

inefficient. MIM structures can confine light at nanometer scale and could show a very high extinction ratio and thus enables modulators with nanometer scale size.

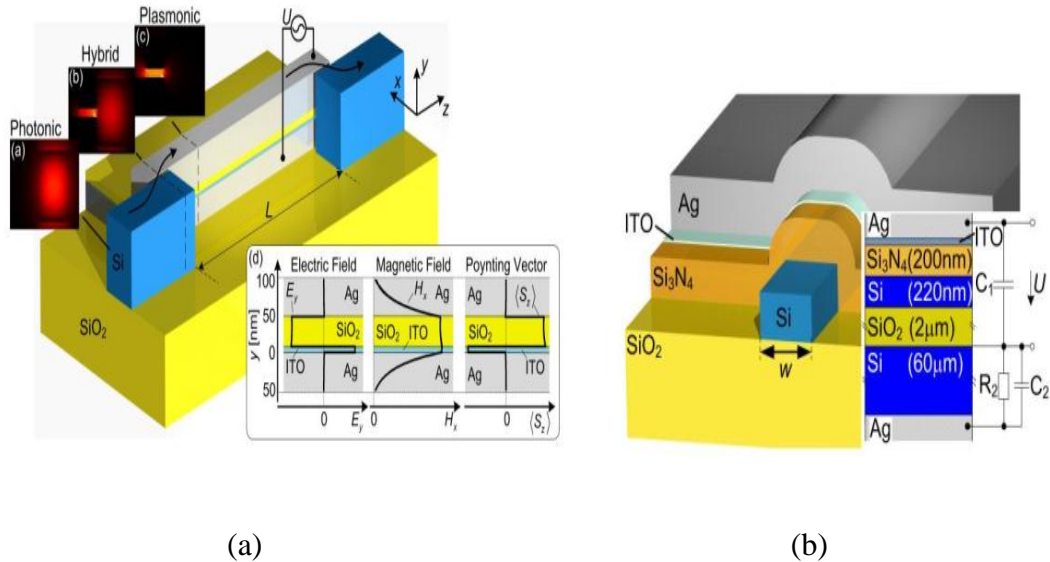


Fig. 1.3 Modulator proposed by Melikyan et al. [5] (a) MIM configuration (b) Proof of principle configuration. Reprinted by permission from “Surface plasmon polariton absorption modulator,” by A. Melikyan, N. Lindenmann, S. Walheim, P. Leufke, S. Ulrich, J. Ye, P. Vincze, H. Hahn, T. Schimmel, C. Koos, W. Freude, and J. Leuthold, 2011, Opt. Express 19, 8855-8869., Copyright 2011 by Optical Society of America.

Atwater and group demonstrated unity order index change in ITO for visible wavelength in case of MOS structure [3]. Ellipsometric measurement showed that an accumulation layer of about 5nm in thickness was formed under a voltage bias. A.P. Vasudev et al. proposed MOS design as illustrated in Fig. 1.2, based on silicon on insulator waveguide with HfO_2 and ITO films [4]. A proof of principle experimental demonstration was reported by Melikyan et al. [5]. Although, the architecture proposed was an MIM configuration, the proof of principle experiment was demonstrated on a silicon nanowire

with multilayer stack of silicon nitride, ITO and silver. The proposed configuration and proof of principle configuration can be seen in Fig. 1.3. The extinction ratio achieved in this experiment was very low ($\sim 1.5 \times 10^{-2}$ dB) [5]. Sorger group experimentally demonstrated a modulator design as depicted in Fig. 1.4. The device structure is integrated with a silicon ridge waveguide where an extinction ratio of 1dB/ μm was achieved [2]. Babicheva et al. analytically discussed few modulator architectures based in transparent conductive oxides [6]. Performance of various investigated modulator architectures is presented in Table 1.

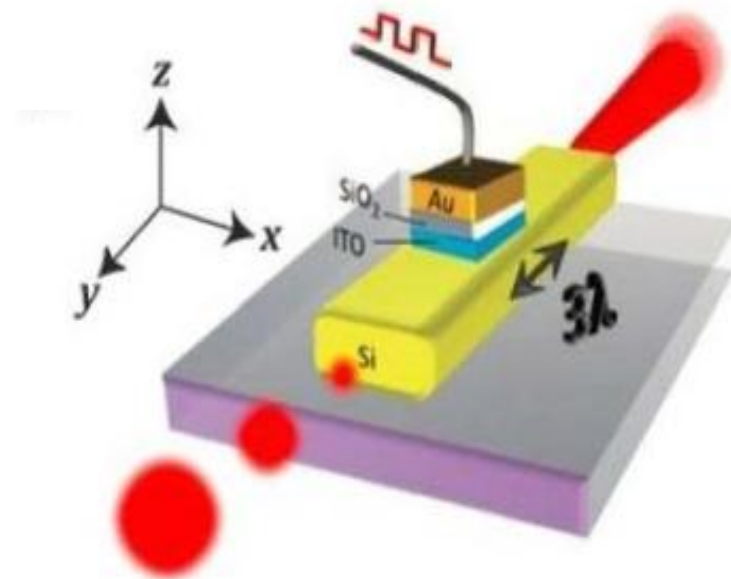


Fig. 1.4 Modulator integrated with SOI waveguide proposed by Sorger group [2]. Reprinted by permission from “Ultra-compact silicon nanophotonic modulator with broadband response,” by V. J. Sorger, N. D. Lanzillotti-Kimura, R. M. Ma, and X. Zhang, 2012, *Nanophotonics*, 1, 17-22., Copyright 2012 by Walter De Gruyter.

Device Type	Extinction Ratio (dB/μm)	Insertion Loss (dB/μm)	Reference
Hybrid plasmonic waveguide	1	0.04	2
Si ridge waveguide (HfO ₂ /ITO)	0.11	0.003	4
Ag/ITO/SiO ₂ /Ag, MIM plasmonic	0.5	Not reported	5
Plasmonic (ITO patterned layer)	3.2	0.8	6

Table 1: Performance of various reported modulator architectures.

1.4 Organization of the Thesis

This thesis is divided into 4 chapters. Chapter 1 introduces the topic and discusses the recent research that has been conducted in the field of plasmonic modulators. Chapter 2 describes the theoretical background of waveguides. It includes discussions on the Eigen mode analysis of planar and rectangular waveguides. Chapter 3 contains design and modeling for the devices examined in this investigation. It describes in detail two proposed device architectures and their analysis. Chapter 4 provides a summary of the thesis.

CHAPTER II

THEORETICAL BACKGROUND

In this chapter the principal of Eigen modal analysis for various waveguide configurations is outlined. Analytical methods for slab waveguides, diffused waveguides and rectangular waveguides are described in detail.

2.1 Modal Analysis

Optical waveguides are the main element of any integrated optical circuit. Light waves travel in waveguides in the form of modes which can be determined by solving Maxwell's equations using relevant boundary conditions. Maxwell's equations are as follows [7]

$$\nabla \times \mathbf{E} = -\mu_o \frac{\partial \mathbf{H}}{\partial t} \quad (2.1)$$

$$\nabla \times \mathbf{H} = \mathbf{J} + \varepsilon_o \frac{\partial \mathbf{E}}{\partial t} \quad (2.2)$$

$$\nabla \cdot \mathbf{D} = \rho \quad (2.3)$$

$$\nabla \cdot \mathbf{B} = 0 \quad (2.4)$$

where \mathbf{E} is electric field intensity vector, \mathbf{H} is magnetic intensity field vector, \mathbf{J} is the current density, ρ is free charge density, μ_o and ε_o are magnetic permeability and electric

permittivity of free space, respectively, \mathbf{B} and \mathbf{D} represent magnetic and electric flux density vectors. \mathbf{J} and ρ are zero for most cases in optics as the material considered are predominantly dielectric in nature and free of sources.

$$\mathbf{D} = \epsilon \mathbf{E} \quad (2.5)$$

$$\mathbf{B} = \mu \mathbf{H} \quad (2.6)$$

with ϵ and μ being the material permittivity and permeability, respectively. Taking curl of equation (2.1), yields the wave equation for the electric field vector. The resultant wave equation is expressed by the following

$$\nabla^2 \mathbf{E} = \epsilon \mu \frac{-\partial^2 \mathbf{E}}{\partial t^2} \quad (2.7)$$

Similarly, we can write

$$\nabla^2 \mathbf{H} = \epsilon \mu \frac{-\partial^2 \mathbf{H}}{\partial t^2} \quad (2.8)$$

As a general solution, the electric field and magnetic field can be written as

$$\mathbf{E} = \mathbf{E}_o \exp(j \mathbf{k} \cdot \mathbf{r}) \exp(j\omega t) \quad (2.9)$$

$$\mathbf{H} = \mathbf{H}_o \exp(j \mathbf{k} \cdot \mathbf{r}) \exp(j\omega t) \quad (2.10)$$

where \mathbf{k} is the wave propagation vector, with a magnitude

$$|\mathbf{k}| = \omega \sqrt{\epsilon \mu} \quad (2.11)$$

2.2 Dielectric Slab Waveguide

The simplest optical waveguide is a planar slab waveguide as shown in Fig. 2.1. It consists of a guiding layer of a higher refractive index, n_f , than the substrate on lower side (n_s) and the cladding layer above it (n_c). Since, the waveguide is infinite in y direction, there will be no spatial variation for the fields along y axis. For propagation along z - axis, electric and magnetic field will vary along x -axis. Refractive indices of the material are chosen to fulfill the following condition.

$$n_f > n_s > n_c .$$

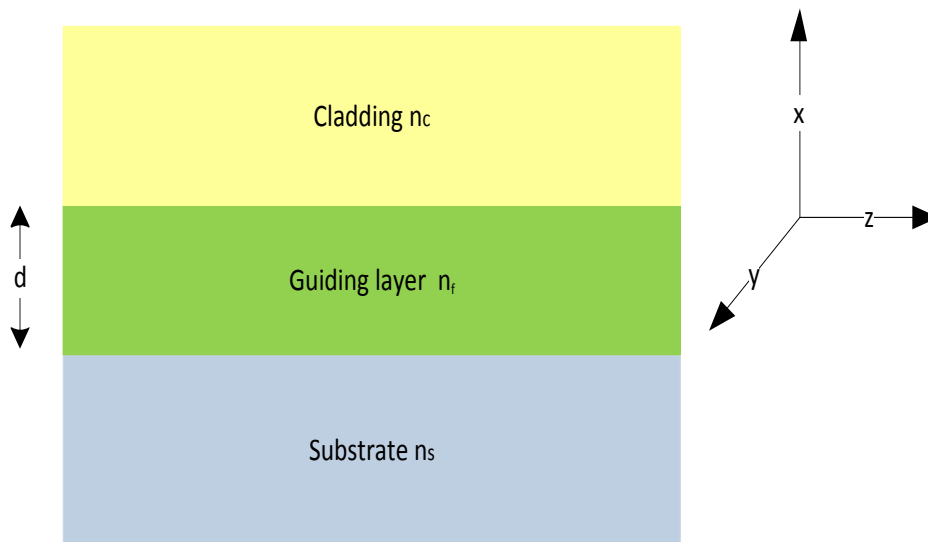


Fig. 2.1 Dielectric slab waveguide structure.

There can be two possible polarizations, namely transverse electric (TE) and transverse magnetic (TM). The transverse electric wave equation can be written in a scalar form as

$$\nabla^2 E_y = k_o^2 n_i^2 E_y \quad (2.12)$$

$$\frac{\partial^2 E_y}{\partial x^2} = (k_o^2 n_i^2 - \beta^2) E_y \quad (2.13)$$

where β is the longitudinal phase constant along the direction of propagation of the optical wave. The wave equation (2.13) can be solved using boundary conditions to obtain the electric field distribution, which can be expressed by the following

$$E_y(x) = \begin{cases} A \exp(-qx) \\ A \left[\cos(hx) - \frac{q}{h} \sin(hx) \right] \\ A \left[\cos(hd) - \frac{q}{h} \sin(hd) \right] \exp[p(x+d)] \end{cases} \quad (2.14)$$

$$q = \sqrt{\beta^2 - n_c^2 k_o^2} \quad (2.15)$$

$$h = \sqrt{n_f^2 k_o^2 - \beta^2} \quad (2.16)$$

$$p = \sqrt{\beta^2 - n_s^2 k_o^2} \quad (2.17)$$

Continuity of tangential components of electric field and magnetic field yields the following Eigen value equation

$$\tan(hd) = \frac{h(p+q)}{h^2 - pq} \quad (2.18)$$

The Eigen value equation is a transcendental equation which can be solved numerically or graphically. Graphical representation of the left hand side (LHS) and the right hand side (RHS) of the equation is shown in Fig. 2.2, and reveal the presence of various possible modes. The field distribution for the first two modes is illustrated in Fig. 2.3.

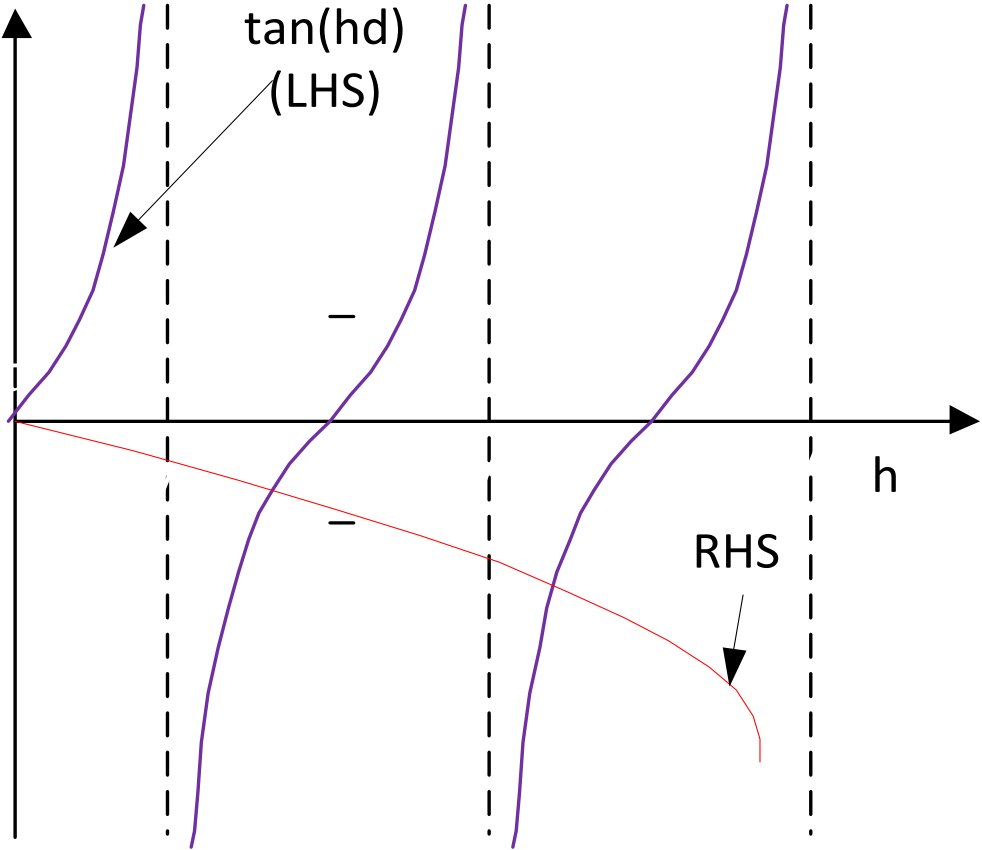


Fig. 2.2 Eigen value equation graphical plot.

Similarly, for the case of TM polarization, the obtained Eigen value equation is

$$\tan(hd) = \frac{h\left(\frac{n_f^2}{n_s^2}p + \frac{n_f^2}{n_c^2}q\right)}{h^2 - \frac{n_f^2}{n_c n_s}pq} . \quad (2.19)$$

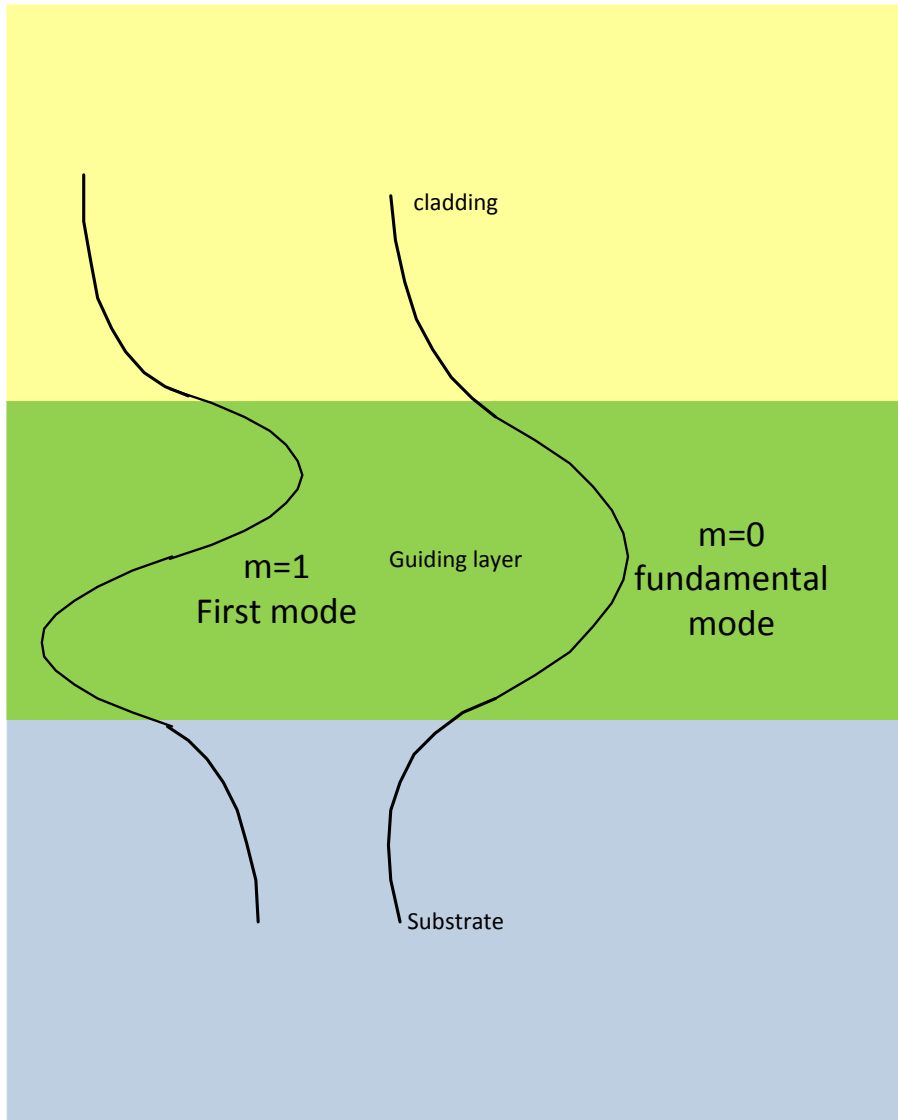


Fig. 2.3 Field distribution of first two TE modes in a slab waveguide.

2.3 Planar Graded Index Waveguides

Diffused waveguides exhibit graded index distribution, where the refractive index varies with depth. Most of the analyses are similar to step index waveguides as discussed in the previous section. There are subtle differences as the boundaries in graded index waveguides are not well defined. Thus, the refractive index is represented by a continuous function $n(x)$ which varies continuously between n_f and n_s .

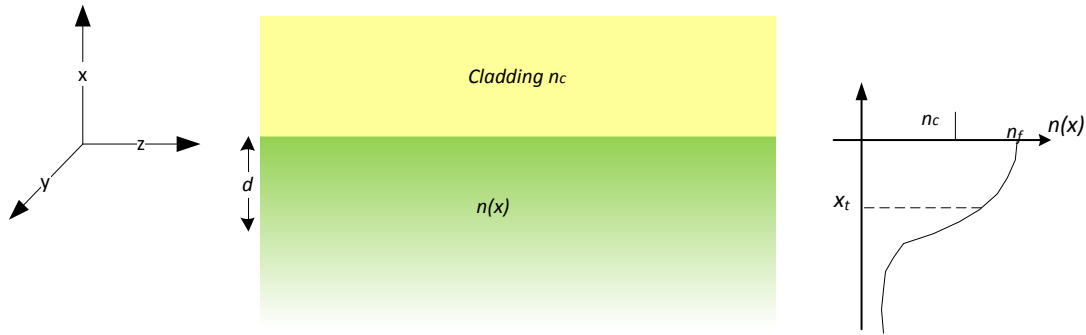


Fig. 2.4 Graded index planar waveguide.

Exact analysis of waveguides having arbitrary refractive index distribution is unlikely. Due to lack of distinct boundary between guiding film and substrate, turning points of a propagating mode are defined. A turning point is similar to the distinct boundary in case of step index waveguide as the mode field distribution beyond the turning point decays exponentially. The field variation in x can be written in a similar way like the step index waveguide, as [7] [8]

$$h_m(x) = k_x(x) = \sqrt{n^2(x)k_0^2 - \beta_m^2} \quad (2.20)$$

$$h_m(x) = k_o \sqrt{n^2(x) - n_{eff}^m{}^2} \quad . \quad (2.21)$$

Turning point divides the waveguide into three regions to the right and left to the turning point. In the vicinity of the turning point it is called a transition zone. The field expressions far away from the turning point decay in a similar fashion to the slab waveguide.

At the turning point

$$h_m(x) \rightarrow 0 \quad (2.22)$$

and in the transition zone

$$n(x) = n_{eff} + (x - x_t) \frac{\Delta n(x)}{\Delta x} \quad (2.23)$$

$$k_x(x) = k_o \sqrt{\left[n_{eff} + (x - x_t) \frac{\Delta n(x)}{\Delta x} \right]^2 - n_{eff}^2} \quad . \quad (2.24)$$

For $(x-x_t) \ll 1$ equation 2.24 reduces to

$$k_x(x) \approx k_o \left[2(x - x_t) \frac{\Delta n(x)}{\Delta x} n_{eff} \right]^{\frac{1}{2}} \quad . \quad (2.25)$$

By writing

$$x_t^\pm = x_t \pm \lim_{\delta x \rightarrow 0} \delta x \quad (2.26)$$

equation (2.25), reduces to

$$k_x(x_t^+) = k_o \lim_{\delta x \rightarrow 0} \left[-2\delta x \frac{\Delta n(x)}{\Delta x} n_{eff} \right]^{\frac{1}{2}} = j\delta k_x \quad (2.27)$$

$$k_x(x_t^-) = k_o \lim_{\delta x \rightarrow 0} \left[-2\delta x \frac{\Delta n(x)}{\Delta x} n_{eff} \right]^{\frac{1}{2}} = \delta k_x \quad (2.28)$$

This shows that a phase shift of $-\pi/2$ occurs at the turning point. The Eigen value integral for graded index waveguide, can be expressed as

$$2 \int_{-x_t}^0 k_o \sqrt{n^2(x) - n_{eff}^m} dx = \left(2m + \frac{3}{2}\right) \pi \quad (2.29)$$

with n_{eff}^m as the effective index of guided mode, and m designates the mode. If the graded index waveguide have two turning points and no clear boundary. then Eigen value integral is given as follows

$$\int_{-x_t}^{x_t} k_o \sqrt{n^2(x) - n_{eff}^m} dx = \left(m + \frac{1}{2}\right) \pi \quad (2.30)$$

2.4 Rectangular Waveguides

Rectangular waveguides are widely used in integrated optics. They can confine the light in both directions across its cross-section. Highest refractive index region forms the core of the waveguide. It is surrounded by lower refractive index regions on all sides. There are several types of rectangular optical waveguides namely channel waveguide, buried waveguide, rib waveguide and ridge waveguide as can be seen in Fig. 2.5.

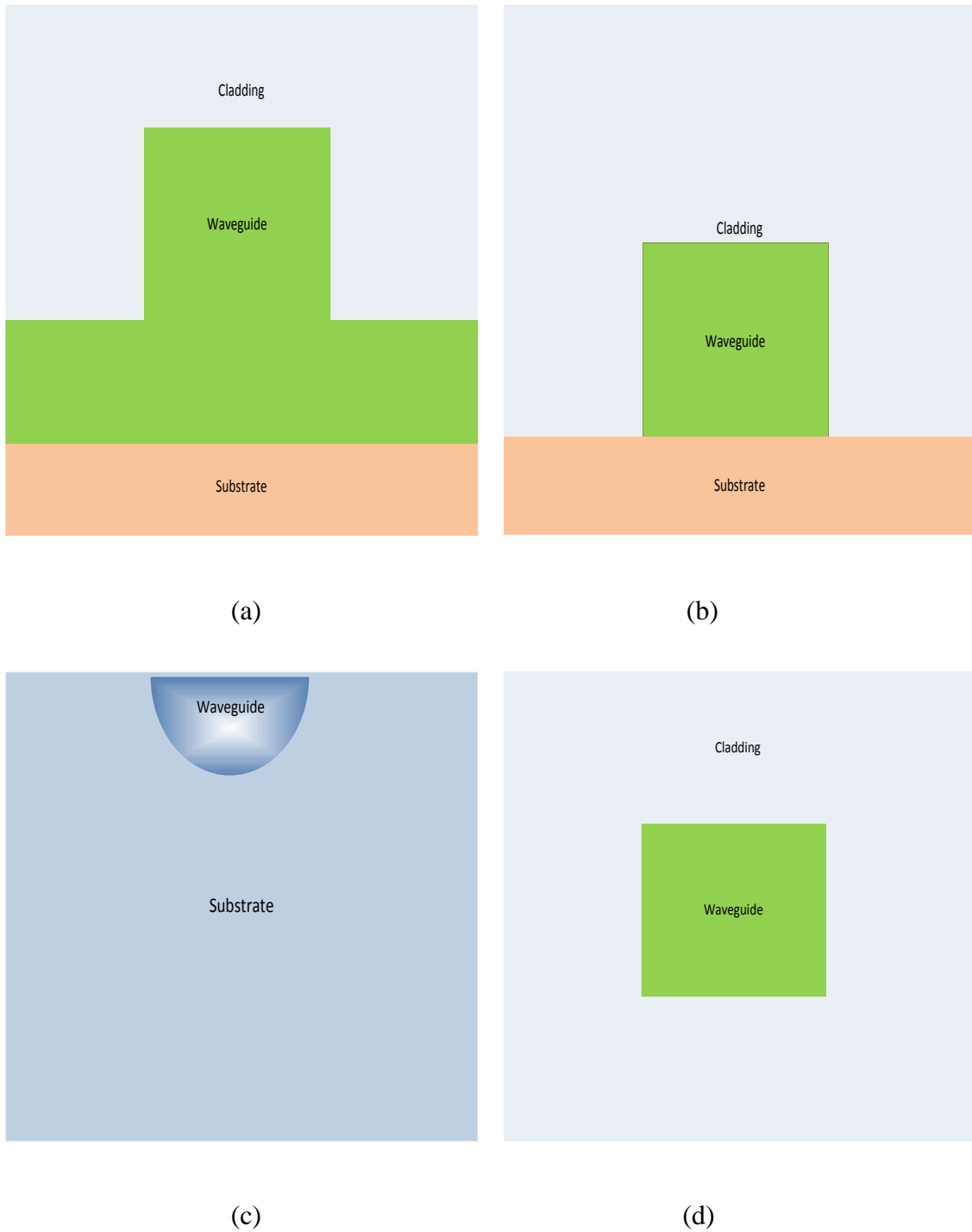


Fig. 2.5 Rectangular waveguides configuration (a) Rib waveguide (b) Ridge waveguide (c) Diffused channel waveguide (d) Buried waveguide.

In this section, an analytical method to analyze rectangular waveguides proposed by E.A.J. Marcatili is described [9]. For a rectangular waveguide as shown in Fig. 2.6, assuming a weakly guiding condition and ignoring the fields in the corner regions, the scalar wave equation can be written in general form as follows

$$\frac{\partial^2 \psi(x, y)}{\partial x^2} + \frac{\partial^2 \psi(x, y)}{\partial y^2} + (n^2 k_o^2 - \beta_m^2) \psi(x, y) = 0 \quad . \quad (2.31)$$

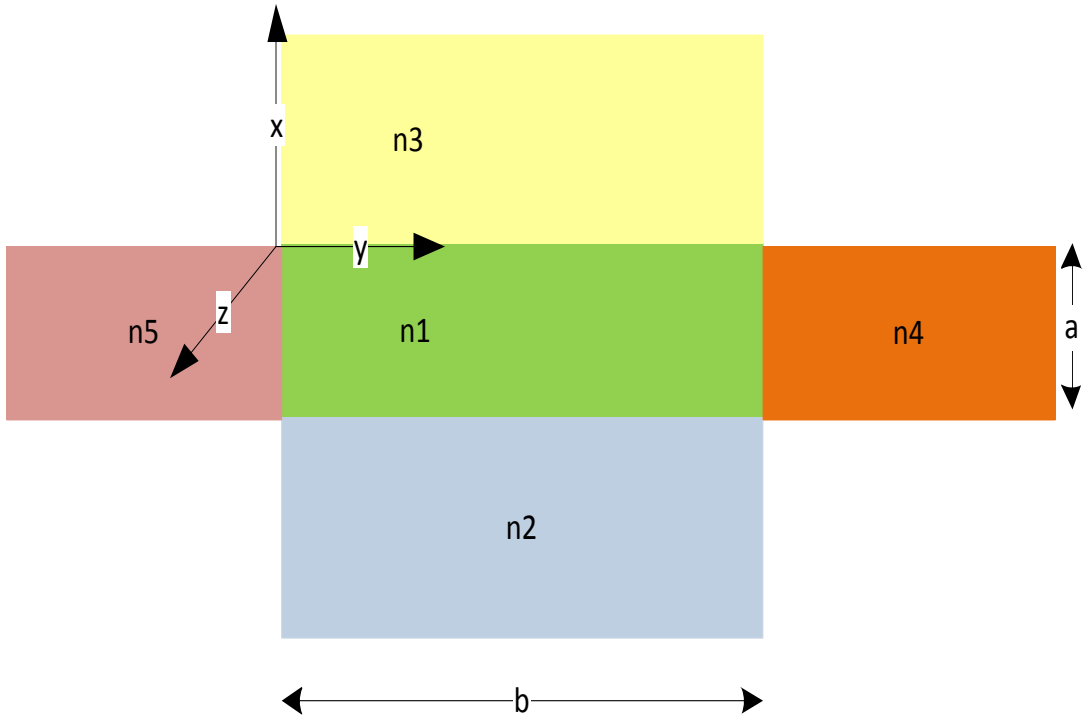


Fig. 2.6 Rectangular waveguide cross section.

Using the product solution approach,

$$\psi(x, y) = X(x)Y(y) \quad (2.32)$$

equation (2.31) can be expressed as

$$\frac{X''}{X} = -n_i^2 k_o^2 + \beta^2 - \frac{Y''}{Y} \equiv -h_x^2 . \quad (2.33)$$

Similarly,

$$\frac{Y''}{Y} = -n_i^2 k_o^2 + \beta^2 + h_x^2 \equiv h_y^2 \quad (2.34)$$

$$\beta^2 = n_1^2 k_o^2 - h_x^2 - h_y^2 . \quad (2.35)$$

As per Marcatili's method, a 3-D waveguide can be analyzed as the combination of two 2-D waveguides. As shown in the previous sections, the field in guiding region is oscillatory, but it decays exponentially in surrounding regions. The field distribution in the corner regions is ignored in this analysis based on the assumption of being very weak to cause any significant contribution in the analysis of field distribution. The field distribution inside the guiding region can then be written as

$$\psi_1 = C_1 \cos(h_x x + \varphi_x) \cos(h_y y + \varphi_y) \quad (2.36)$$

where φ_x and φ_y are the phase parameters.

Expressions for the field variation in each region can be defined, and by applying boundary conditions the transverse wave vectors could be determined.

$$\psi_2 = C_2 \cos(h_y y + \varphi_y) e^{\gamma_2(x+a)} \quad (2.37)$$

$$\psi_3 = C_3 \cos(h_y y + \varphi_y) e^{-\gamma_3 x} \quad (2.38)$$

$$\psi_4 = C_4 \cos(h_x x + \varphi_x) e^{-\gamma_4 (y-b)} \quad (2.39)$$

$$\psi_5 = C_5 \cos(h_x x + \varphi_x) e^{\gamma_5 y} \quad (2.40)$$

where γ_j are transverse wavenumbers, and subscript j identifies the region. The various parameters C_j , φ_j , γ_j , h_x and h_y which are related by the following equations

$$\gamma_2^2 = h_y^2 + \beta^2 - k_o^2 n_2^2 \quad (2.41)$$

$$\gamma_3^2 = h_y^2 + \beta^2 - k_o^2 n_3^2 \quad (2.42)$$

$$\gamma_4^2 = h_x^2 + \beta^2 - k_o^2 n_4^2 \quad (2.43)$$

$$\gamma_5^2 = h_x^2 + \beta^2 - k_o^2 n_5^2 \quad (2.44)$$

can be determined using the boundary conditions along horizontal and vertical interfaces. The boundary conditions yield the final Eigen value equations. The modes in the rectangular waveguides can be designated as E^x and E^y modes. E^x modes can be considered as TE polarized for waveguide thickness ' b ' and TM polarized with waveguide thickness ' a '. Thus Eigen value equations can be expressed as

$$\tan(h_y b) = \frac{h_y (\gamma_4 + \gamma_5)}{h_y^2 - \gamma_4 \gamma_5} \quad (2.45)$$

$$\tan(h_x a) = \frac{h_x \left(\frac{n_1^2}{n_2^2} \gamma_2 + \frac{n_1^2}{n_3^2} \gamma_3 \right)}{h_x^2 - \frac{n_1^2}{n_2 n_3} \gamma_2 \gamma_3} . \quad (2.46)$$

The phase parameters are given by following equations

$$\tan(\varphi_x) = -\frac{n_3^2 h_x}{n_1^2 \gamma_3} \quad (2.47)$$

$$\tan(\varphi_y) = -\frac{\gamma_5}{h_y} . \quad (2.48)$$

Similarly, E^y modes can be considered as TE polarized for waveguide thickness 'a' and TM polarized with waveguide thickness 'b'. Eigen value equations can be described as

$$\tan(h_y b) = \frac{h_y \left(\frac{n_1^2}{n_5^2} \gamma_5 + \frac{n_1^2}{n_4^2} \gamma_4 \right)}{h_y^2 - \frac{n_1^2}{n_5 n_4} \gamma_5 \gamma_4} \quad (2.49)$$

$$\tan(h_x a) = \frac{h_x (\gamma_3 + \gamma_2)}{h_x^2 - \gamma_3 \gamma_2} \quad (2.50)$$

and phase parameters are given by,

$$\tan(\varphi_y) = -\frac{n_5^2 h_y}{n_1^2 \gamma_5} \quad (2.51)$$

$$\tan(\varphi_x) = -\frac{\gamma_3}{h_x} . \quad (2.52)$$

These equations can then be solved to find the mode field distribution. Field profiles for first two E^x and E^y modes are shown in Fig. 2.7.

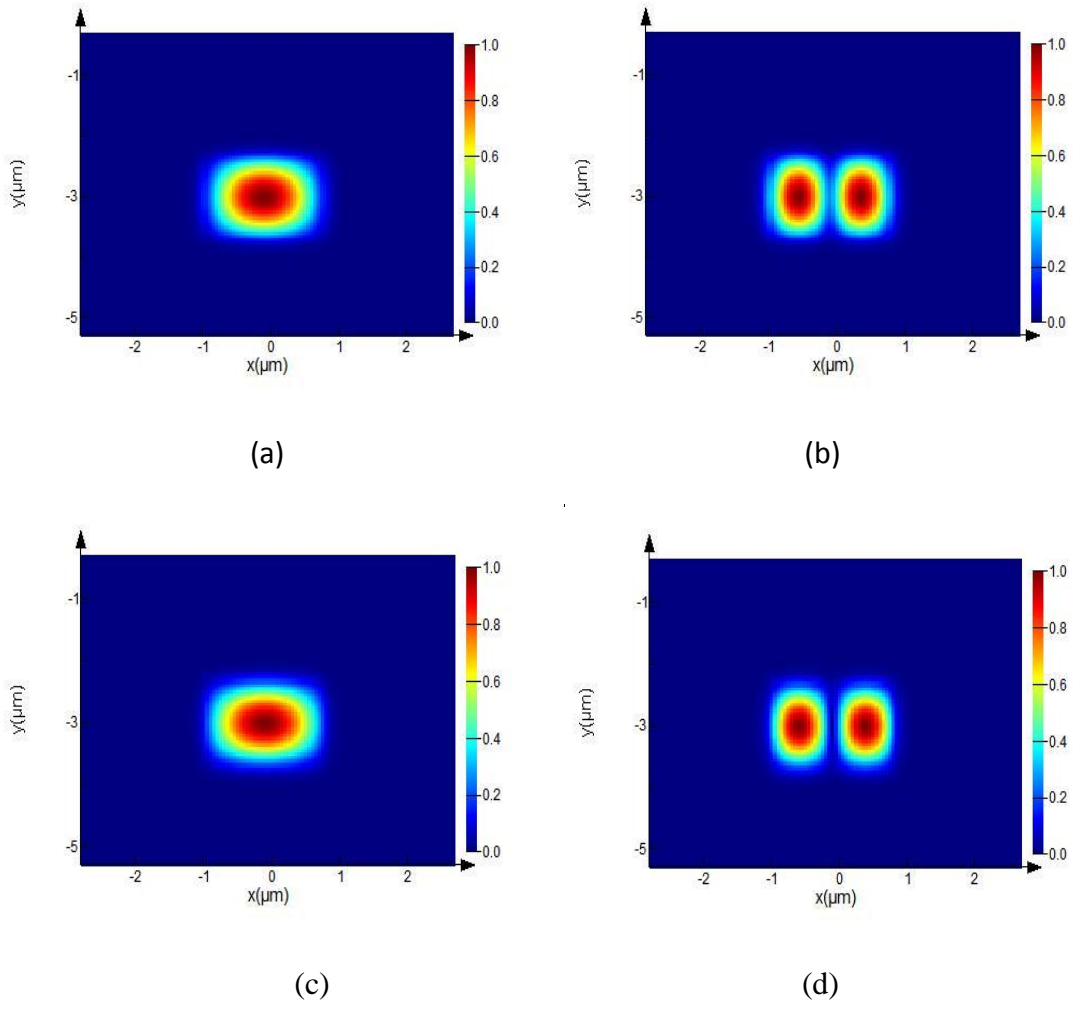


Fig. 2.7 Mode field profiles in rectangular waveguide for (a) E_{00}^x mode (b) E_{10}^x mode (c) E_{00}^y mode (d) E_{10}^y mode.

CHAPTER III

DEVICE ARCHITECTURE AND SIMULATION

The goal of this effort is to develop an efficient electro-absorption modulator in lithium niobate. Modeling of the titanium diffused lithium niobate waveguides is discussed in detail in section 3.1. The proposed device architectures are described in section 3.2. Modeling of the optical properties of ITO which acts as an active material in the device is covered in section 3.3. Coupling to the TiO₂ film which is an important aspect in the proposed device operation is presented in section 3.4. Finally, the results and device performance are detailed out in section 3.5.

3.1 Diffused Channel Waveguide Modeling

Optical waveguides in lithium niobate (LN) are predominantly formed by titanium indiffusion. To begin with, a titanium film is deposited over a certain width on lithium niobate substrate. The width and thickness of the film define the modes that the waveguide will allow. The sample is then kept at elevated temperature of around a 1000°C for several hours. Heating facilitates the thermal diffusion of titanium atoms into the lithium niobate substrate to form a diffused channel waveguide.

Thus, the formed waveguide shows a graded index distribution with refractive index variation along both lateral direction and depth. In order to model the phenomenon, the

diffused titanium atom concentration variation is described in terms of spatial coordinates [10], [11].

The refractive index change is brought about by the diffusion of titanium atoms. Concentration profile can be described based on the diffusion model. Using $c(x,z)$ for the titanium concentration profile in lithium niobate for a given set of coordinate axes as shown in Fig. 3.1, it can be defined using following set of equations

$$c(x, z) = c_o f(z) g(x) \quad (3.1)$$

$$f(z) = \frac{1}{2} \left(\operatorname{erf} \left[\frac{w}{2D_h} \left(1 + \frac{2z}{w} \right) \right] \operatorname{erf} \left[\frac{w}{2D_h} \left(1 - \frac{2z}{w} \right) \right] \right) \quad (3.2)$$

$$g(x) = \exp \left(-\frac{x^2}{D_v^2} \right) \quad (3.3)$$

where c_o is surface concentration, w is the width of waveguide D_h , D_v are diffusion lengths along horizontal and vertical directions, respectively.

The concentration profile can further be used to estimate the refractive index profile in the diffused waveguide. The overall Ti diffused channel waveguide refractive index can then be expressed as

$$n_{o,e}(\lambda, x, z) = n_{o,e}(\lambda) + \Delta n_{o,e}(\lambda, x, z) \quad (3.4)$$

$n_{o,e}(\lambda)$ is the bulk LN refractive index at the operating wavelength λ , and $\Delta n_{o,e}(\lambda, x, z)$ is the induced refractive index change due to titanium in-diffusion. Subscript ‘ o ’ represents ordinary refractive index and ‘ e ’ denotes extra-ordinary refractive index.

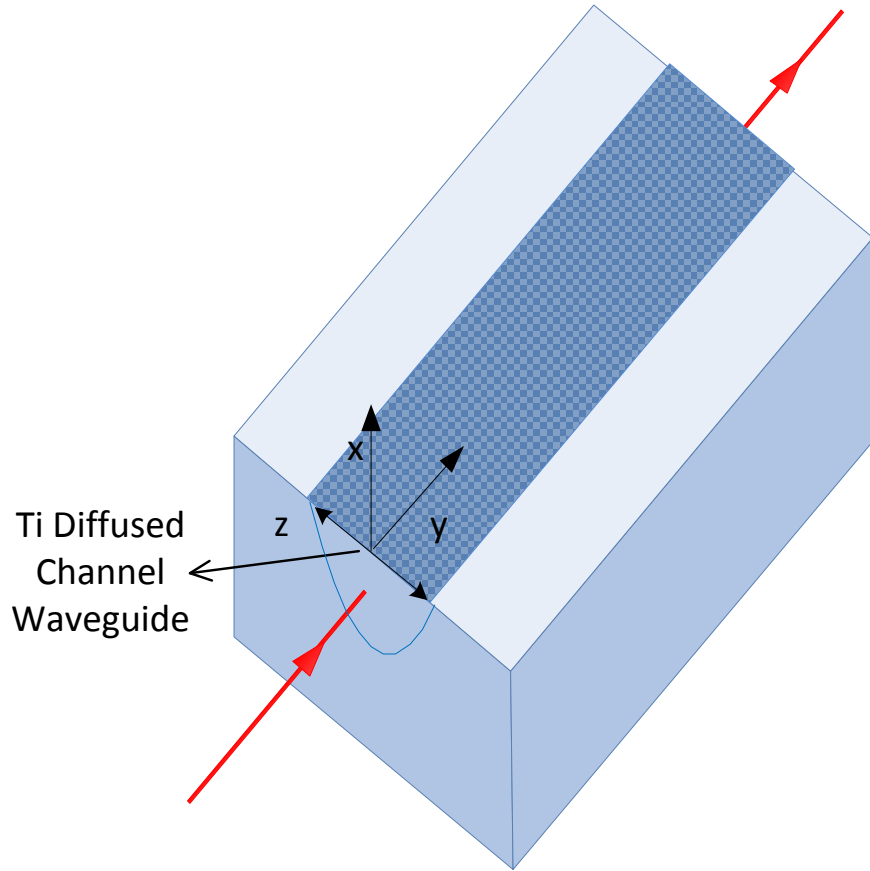


Fig. 3.1 Ti diffused channel waveguide in lithium niobate substrate.

The ordinary and extra-ordinary refractive index of lithium niobate depends on the operating wavelength and can be computed using Sellemeier's dispersion equations [12].

$$n_o^2 = 4.9048 - \frac{0.11768}{0.0475 - \lambda^2} - 0.027169 \lambda^2 \quad (3.5)$$

$$n_e^2 = 4.582 - \frac{0.099169}{0.044432 - \lambda^2} - 0.02195 \lambda^2 . \quad (3.6)$$

The induced refractive index changes are given by the product of dispersion factor and distribution function which depends on the titanium concentration profile [11]

$$\Delta n_{o,e}(\lambda, x, z) = d_{o,e}(\lambda)h_{o,e}(x, z). \quad (3.7)$$

The dispersion factor for ordinary and extra-ordinary refractive indices are given by different equations as described below

$$d_o(\lambda) = \frac{0.67\lambda^2}{\lambda^2 - 0.13} \quad (3.8)$$

$$d_e(\lambda) = \frac{0.839\lambda^2}{\lambda^2 - 0.0645}. \quad (3.9)$$

The distribution function is given by

$$h_{o,e}(x, z) = (F_{o,e}c(x, z))^{\gamma_{o,e}} \quad (3.10)$$

where $F_{o,e}$ is the distribution constant and $\gamma_{o,e}$ is the power distribution factor . Typically, $F_o=1.3 \times 10^{-25} \text{ cm}^3$, $F_e=1.2 \times 10^{-23} \text{ cm}^3$, $\gamma_o=0.55$, $\gamma_e=1$ for titanium diffusion in LN.

Another important parameter which defines the refractive index profile of the diffused waveguide is the thickness of the deposited titanium film before diffusion. Film thickness ‘ t ’ and width ‘ w ’, shown in Fig. 3.2, dictates the number of modes a waveguide can support. The surface concentration constant ‘ c_o ’ and Ti film thickness ‘ t ’, can be related by the following equations

$$c_o = \frac{t C_l}{\sqrt{\pi} D_v} \quad (3.11)$$

$$C_l = \frac{\rho N_A}{A} \quad (3.12)$$

where ρ and A are the density and the atomic mass of titanium respectively, and N_A is the Avogadro number ($\rho = 4.51 \text{ g/cm}^3$, $A = 47.9 \text{ g/mol}$, $C_l = 5.67 \cdot 10^{22} \text{ cm}^{-3}$).

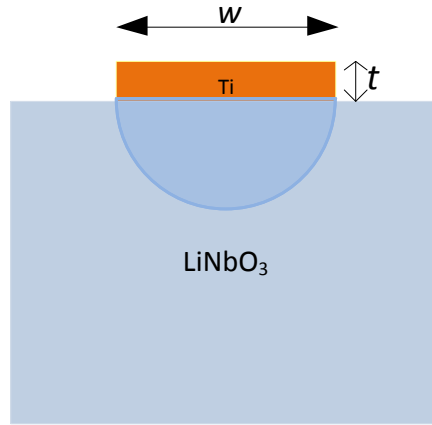


Fig. 3.2 Cross sectional view of diffused channel waveguide with titanium film.

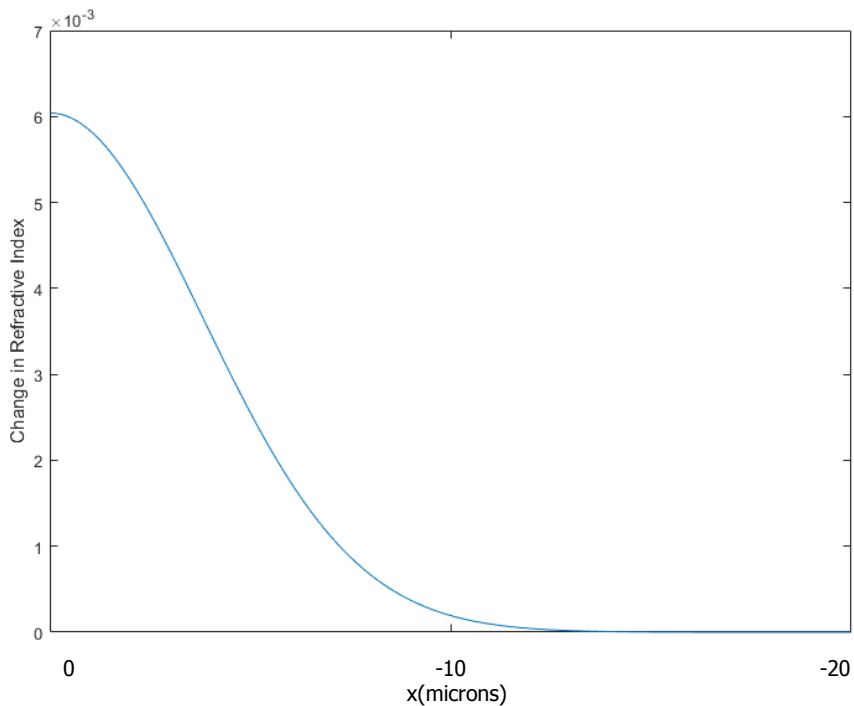
The diffusion lengths (vertical and lateral) depend upon the temperature at which the diffusion is being carried out and the time required for diffusion [13]. Thus they can be defined as follows,

$$D_h = \sqrt{\tau D_h^0 e^{\frac{-T_0}{T}}} \quad (3.13)$$

$$D_v = \sqrt{\tau D_v^0 e^{\frac{-T_0}{T}}} \quad (3.14)$$

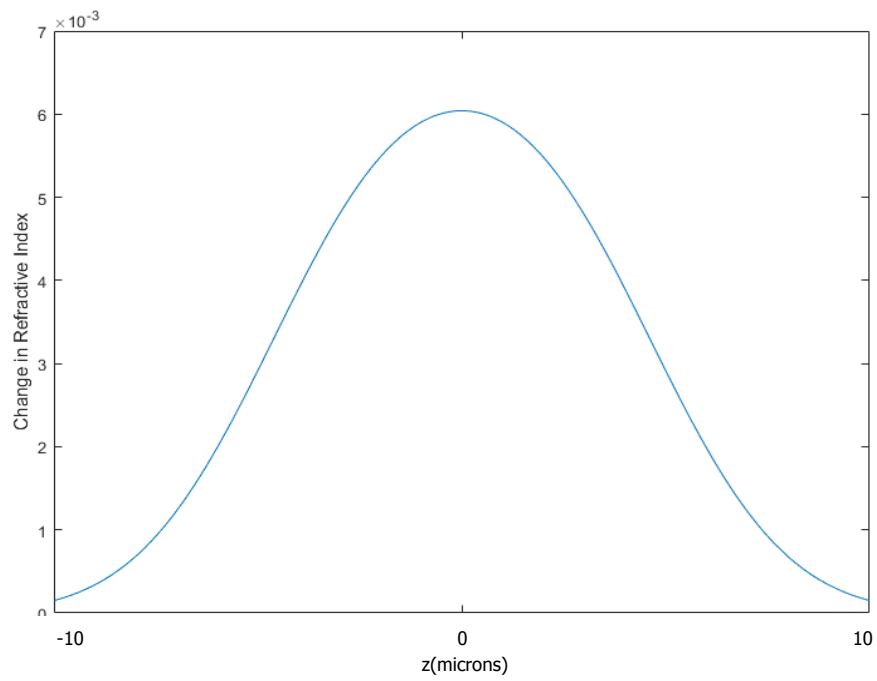
where τ is the diffusion time, T is the temperature at which diffusion is carried out, D_v^o and D_h^o are the diffusion constant in vertical and lateral directions, T_o is the temperature coefficient (T_o is typically of the order of 2.9×10^4 K). Diffusion constant is specific to a given substrate, dopant and axis of the crystal. Since lithium niobate is anisotropic, the values of diffusion coefficient along lateral and vertical directions are different.

It is evident from the above analysis that titanium concentration profile is a Gaussian function with depth. Refractive index profile along the depth depends on the power distribution factor as well. Fig. 3.3 illustrates the refractive index changes and profile for an X-cut lithium niobate substrate and y propagating ordinary wave.

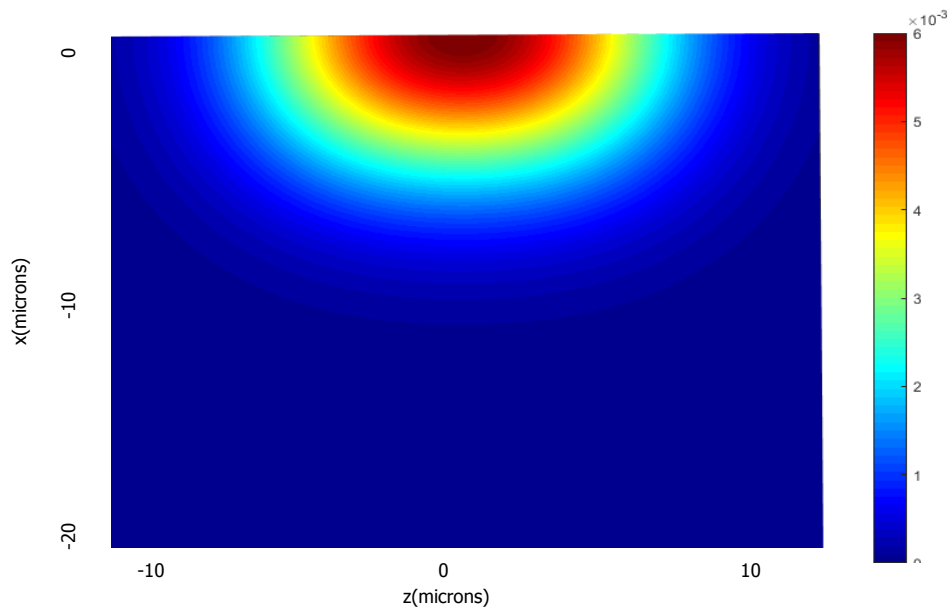


(a)

Fig. 3.3 Refractive index change due to Ti diffusion (a) along depth (b) along lateral direction (c) 2-D profile.



(b)



(c)

Fig. 3.3 Continued.

3.2 Proposed Modulator Architecture

In this section, two modulator architectures integrated with a Ti diffused lithium niobate waveguide are described. ITO is used as an active material for modulation. Refractive index of ITO changes in the presence of electric field owing to increased free charge carriers density. Thus, it can be effectively used for electro-absorption modulation.

Architecture 1 as depicted in Fig. 3.4 consists of a stack of ITO, SiO₂ and Au deposited over the diffused waveguide. SiO₂ film provides insulation and thus forms a metal oxide semiconductor (MOS) capacitor. ITO and SiO₂ films are 10nm each and Au acts as a gate, with electric field applied between Au and ITO. A device based on this architecture is very easy to fabricate but it suffers from low modulation. Mode size in titanium diffused waveguides is of the order of 7-8μm, which leads to low light matter interaction with the active material [14].

Change in material refractive index doesn't necessarily ensure high modulation efficiency. For efficient modulation, a large change in effective index of the propagating mode is required. This requires a well confined modal field near the surface of waveguide and a strong light matter interaction (LMI) of the mode with ITO. Although, Ti diffused waveguides are one of the best choices for optical communications as they have very low loss and very high coupling efficiency with optical fiber, their large modal size becomes a major challenge to achieve strong LMI with ITO, thus leading to low modulation efficiency.

A novel alternative configuration (Architecture 2) for enhancing LMI is also proposed, which can overcome this limiting factor and produce high modulation efficiency. The modulator design is simple and easy to integrate with titanium diffused waveguides on lithium niobate. It consists of a stack of ITO/SiO₂/Au and includes a TiO₂ film extended partially over the waveguide. The film thickness for TiO₂ over ITO is 350nm and over the rest of waveguide is 380nm. ITO, SiO₂ and Au are 10nm thick each, $L_1=20\mu\text{m}$ and $L_2=65\mu\text{m}$ as shown in Fig. 3.5. ITO acts as the active material and the added TiO₂ film enhances the light matter interaction for the propagating mode. Au is used as an electrode to provide electric field across the stack with ITO serving as a ground terminal. ITO changes refractive index under application of voltage bias across the stack, similar to Architecture1. A detailed description of the optical properties of ITO is given in later sections.

Since, without a high LMI, an efficient modulator is not possible. TiO₂ film is employed to enhance LMI. TiO₂ has a higher refractive index than the overall refractive index of titanium diffused channel waveguide. Thus, TiO₂ film which is deposited over the waveguide will shift the optical field closer to the surface of the waveguide. Thickness of the film is optimized to achieve high field density near the surface of the waveguide. Due to the introduction of the TiO₂ film, effective mode index changes occur and thus the coupling length becomes an important parameter. Placement of the modulator structure (ITO/SiO₂/Au stack) with respect to the TiO₂ film will depend on the coupling length. An optimized placement will give the best performance.

Since the modulator structure is on the surface of the titanium diffused waveguide, only TM mode will interact with ITO and exhibit optical intensity modulation. TE mode will show minimal interaction. Thus, analysis of only the TM mode is discussed for device performance in later sections. The coupling characteristics of the waveguide mode with TiO_2 film will be detailed in section 3.4.

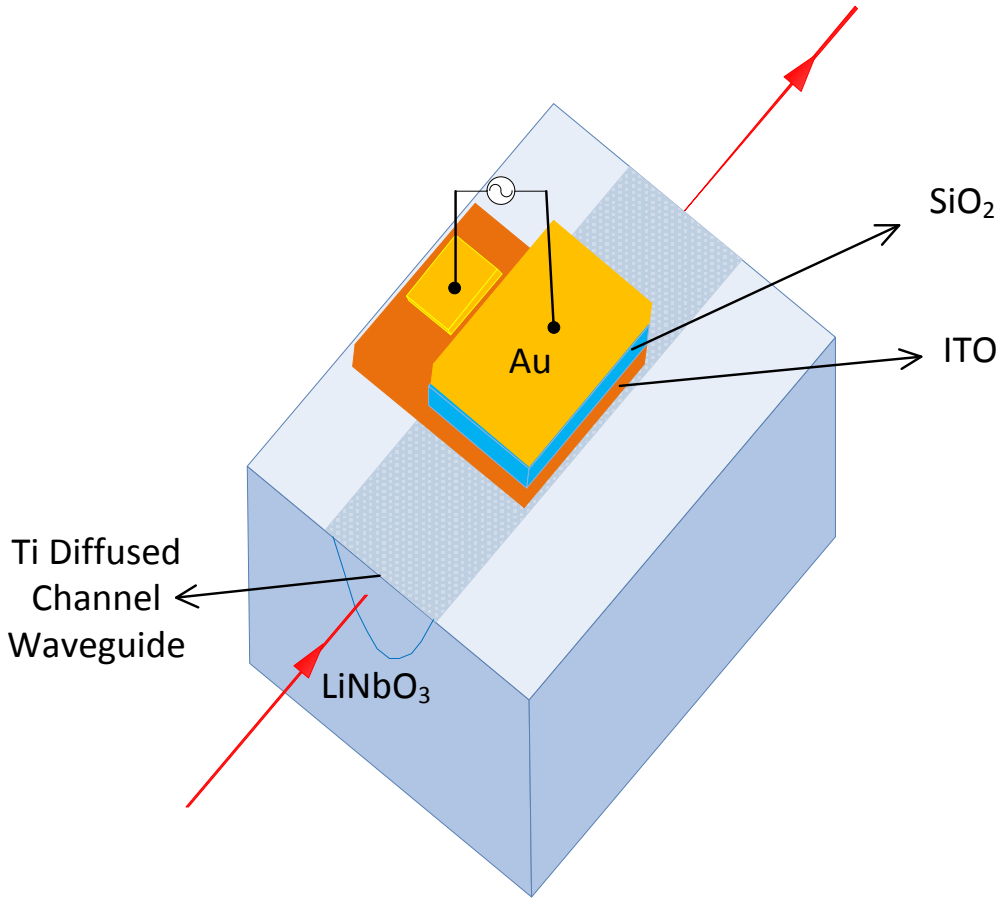
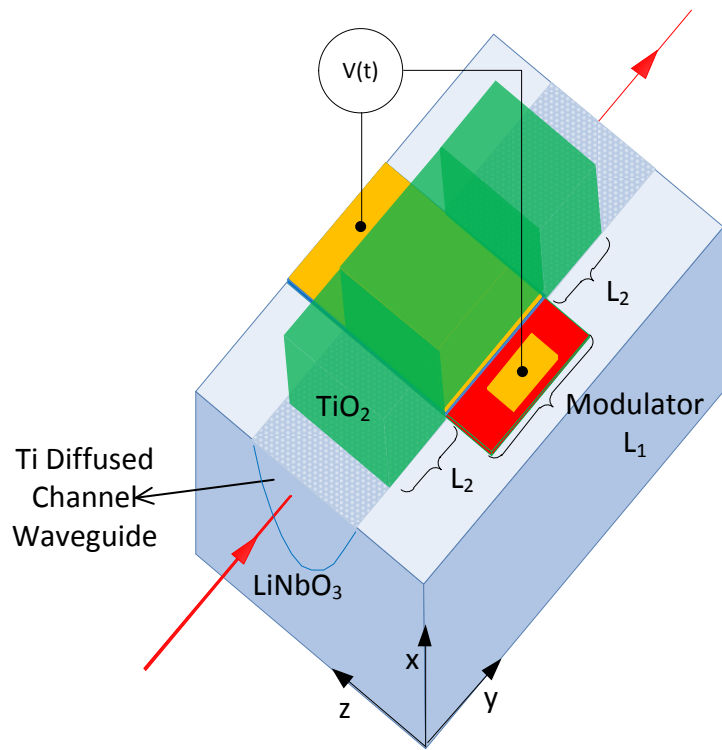
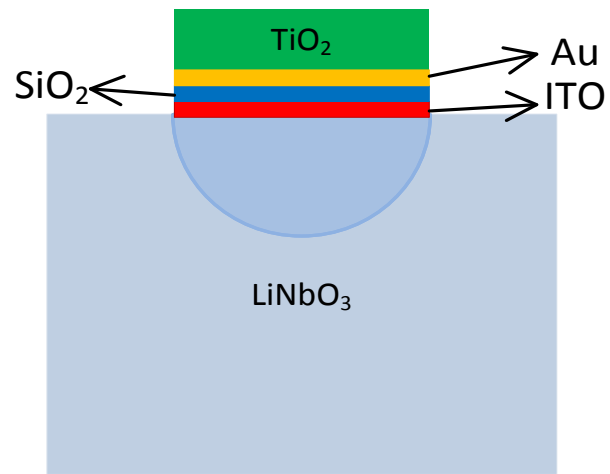


Fig. 3.4 Architecture 1: Modulator configuration integrated with Ti diffused waveguide.



(a)



(b)

Fig. 3.5 Architecture 2 modulator configuration (a) Perspective view (b) Cross sectional view.

3.3 Optical Properties of Indium Tin Oxide (ITO)

Recent research suggests the potential benefits ITO offers for use in active photonic devices. It has unique electro-optic properties which are highly tunable. Atwater and group have showed experimentally that refractive index of ITO can show a unity order refractive index change by applying sufficient voltage bias [3]. ITO can also function in epsilon near zero (ENZ) regime, which makes it an attractive choice to be used for electro-optic modulators.

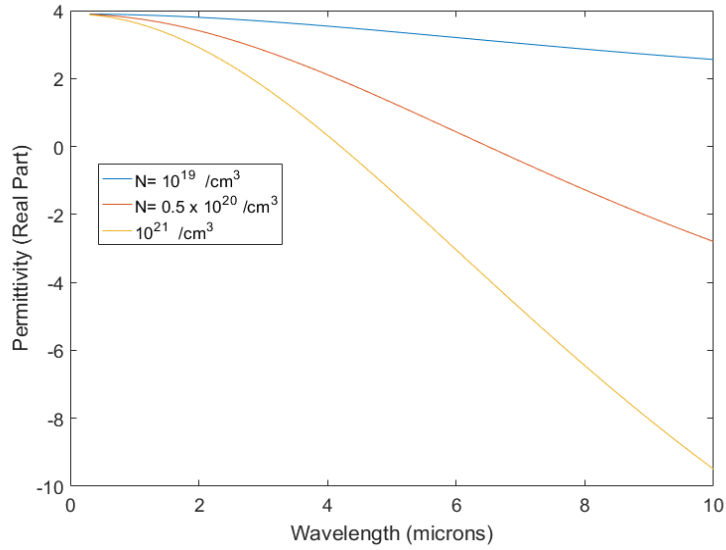
As the refractive index of ITO can be tuned, it can effectively be used to change the effective mode index of the propagating mode. It has the possibility of using it for both optical intensity and phase modulators. The permittivity of the ITO can be tuned by changing the free charge carriers concentration by means of applying a voltage bias. The deposition conditions can also be altered to get a desired initial carriers concentration. Permittivity of ITO can be effectively described using the Drude model [4]

$$\epsilon = \epsilon_{\infty} - \frac{\omega_p^2}{\omega^2 + i\omega\gamma} \quad (3.15)$$

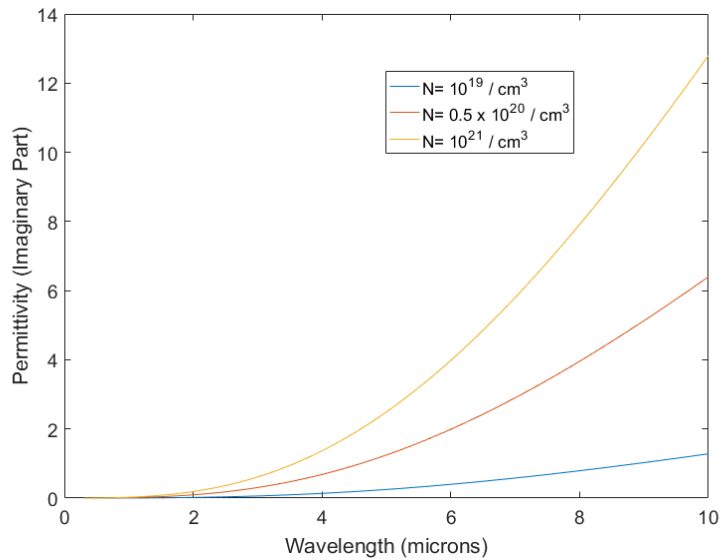
$$\omega_p^2 = \frac{ne^2}{\epsilon_o m^*} \quad (3.16)$$

where $\epsilon_{\infty} = 3.9$ is the high frequency dielectric constant, $\gamma = 1.8 \times 10^{14}$ is the electron scattering rate, ω_p is the plasma frequency, and ω is the frequency of light. $m^* = 0.35 m_e$ is the electron effective mass, n , e , ϵ_o are the free carriers density, fundamental charge and the permittivity of free space, respectively. The plots in Fig. 3.6 illustrate the

permittivity and refractive index variation of the ITO as predicted by the Drude model with free charge carriers density as a parameter.

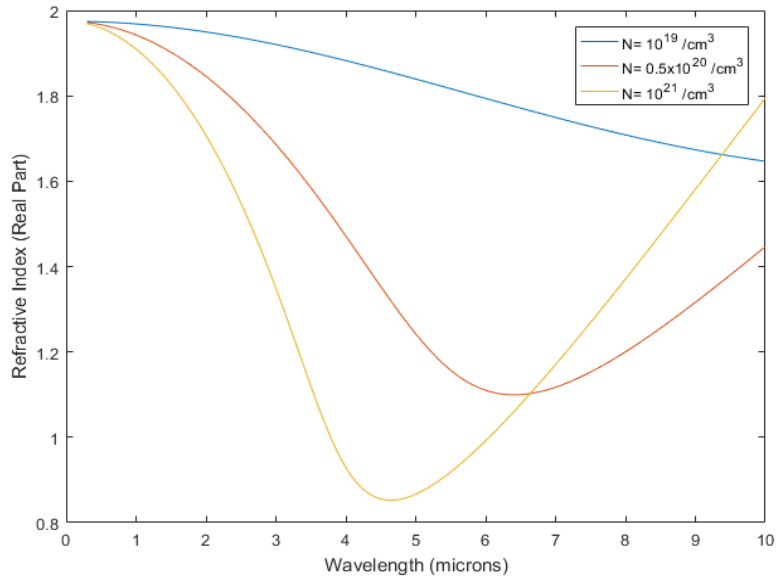


(a)

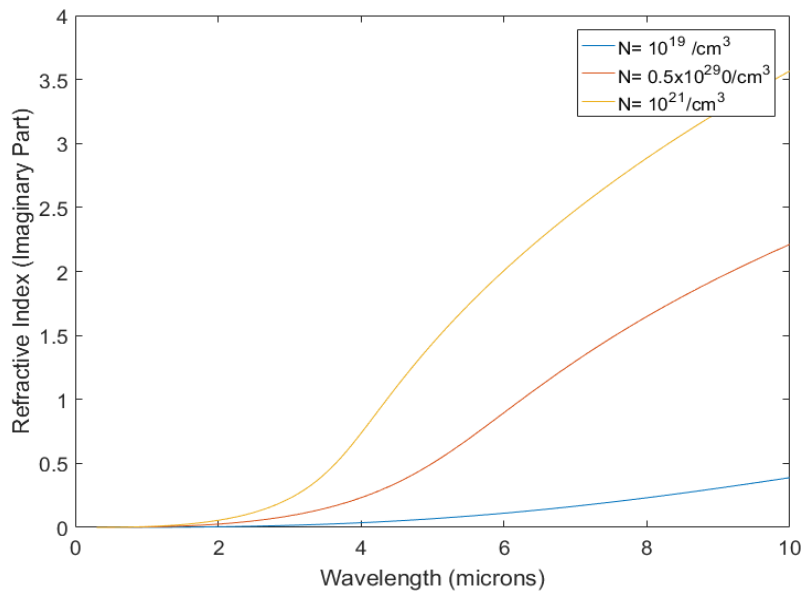


(b)

Fig. 3.6 Optical properties of ITO as a function of wavelength (a) Permittivity real part (b) Permittivity imaginary part (c) Refractive index real part (d) Refractive index imaginary part.



(c)



(d)

Fig. 3.6 Continued.

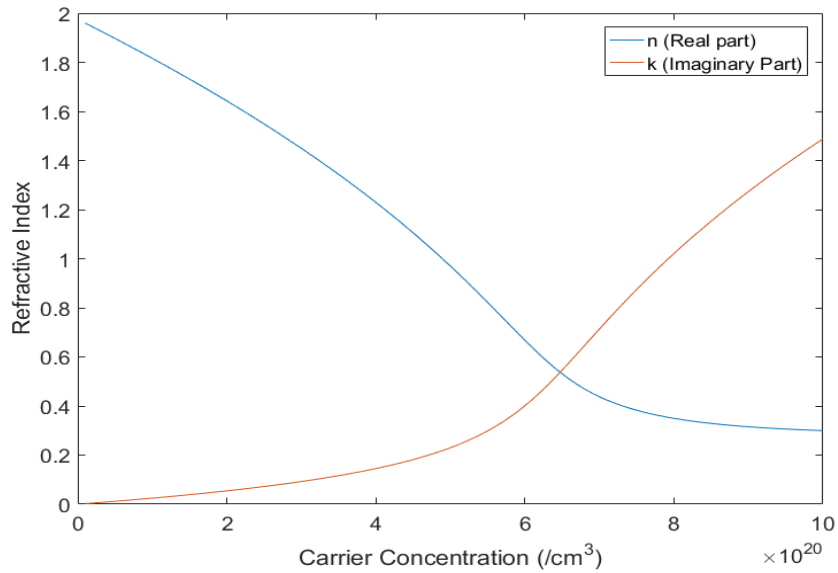


Fig. 3.7 ITO refractive index vs. carriers concentration.

The device architectures described in previous sections are designed to operate at telecommunications wavelength ($1.55\mu\text{m}$). Fig. 3.7 illustrates refractive index variation (real and imaginary part) with free charge carriers density for $1.55\mu\text{m}$ wavelength. ITO films can be integrated with a diffused waveguide type device design and it is possible to achieve optical intensity modulation. However, it is not necessary that modulation will be very efficient but it can be significantly enhanced by the careful design of device architecture. The device design should be such that with the change in refractive index of ITO, effective mode index of the propagating mode can also be changed significantly. This requires very high light matter interaction of propagating mode with ITO or else there will be a minimal change. In case of plasmonic and slot waveguides, light can be confined in a sub-wavelength region and thus achieve high optical intensity modulation.

The proposed alternative device design configuration (Architecture 2) presented in this investigation is aimed at enhancing the mode field response.

3.4 Coupling to TiO₂

Hybrid waveguide (Ti Diffused and TiO₂ film) as shown in Fig. 3.8, was simulated using the finite difference time domain (FDTD) algorithm (Lumerical FDTD solutions). Refractive index of TiO₂ film is larger than the overall index of Ti diffused waveguide [15]. This enables shifting the electric field of the guided optical mode towards the surface of the waveguide. After maximum coupling from Ti diffused waveguide to hybrid waveguide, the optical field of the guided mode appears predominantly near the surface.

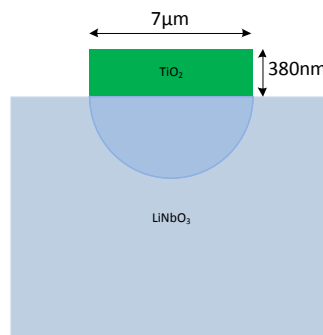
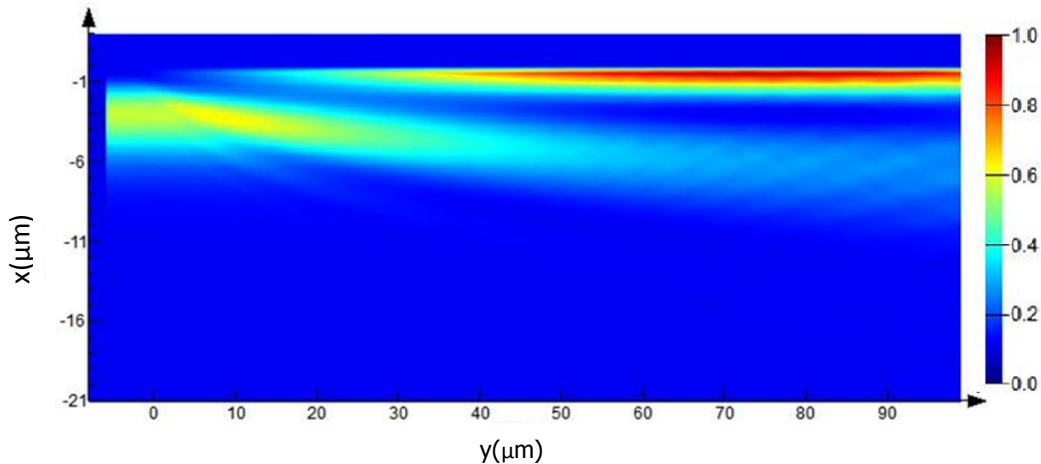


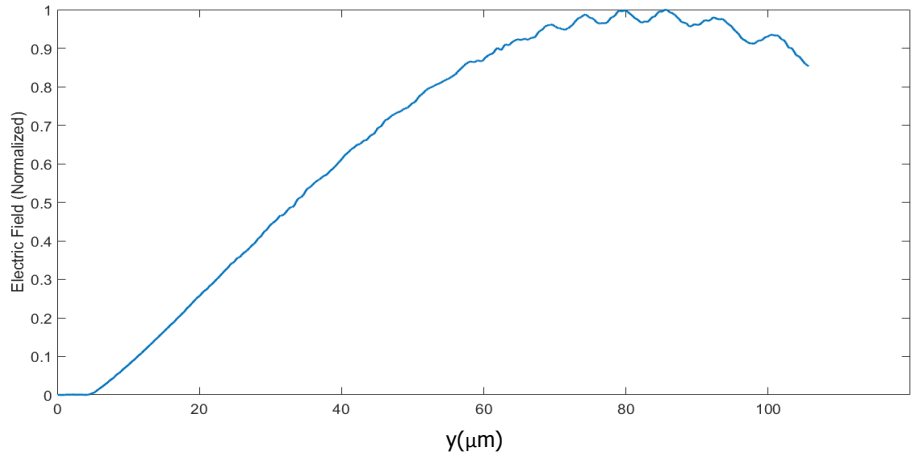
Fig. 3.8 Cross section of the hybrid TiO₂ and Ti diffused waveguide.

As such, the TiO₂ film enables higher interaction between the optical field and ITO film and ultimately improves the modulation efficiency of the device. Fig. 3.9 shows the power coupling from Ti diffused waveguide to 380 nm TiO₂ film. Due to the coupling characteristics of the hybrid waveguide, positioning of the modulator layered stack

becomes a relevant parameter. The effect of TiO_2 film on the propagating guided mode saturates after traversing $65\mu\text{m}$ of travel length. This makes it an optimized position to integrate the modulator with the waveguide. Since, field density in the hybrid waveguide is highest at the surface of LN; ITO/ SiO_2 /Au stack should be placed right above the surface of Ti diffused waveguide as in the case of Architecture 2.



(a)



(b)

Fig. 3.9 Electric field distribution for LN- TiO_2 hybrid waveguide with propagation distance (a) lateral cross-section (b) at LN waveguide surface.

3.5 Results and Discussion

The optical intensity is modulated by changing the free carriers concentration in ITO under applied voltage bias. The applied voltage induces an accumulation of free charge carriers at the SiO₂-ITO interface which in turn changes the effective index of the propagating mode.

Firstly, the performance of modulator architecture without TiO₂ film (Architecture 1) as depicted in Fig. 3.4 is discussed. TM polarized light is launched into the Ti diffused LN waveguide which excites fundamental TM mode, as illustrated in Fig. 3.10. The TM mode then interacts with the modulator stack. Modal analysis for the modulator configuration is carried out to search for an optimized performance of the device. The modes of modulator stack are observed for the maximum and the minimum absorption with varying accumulated charge carriers density as the parameter.

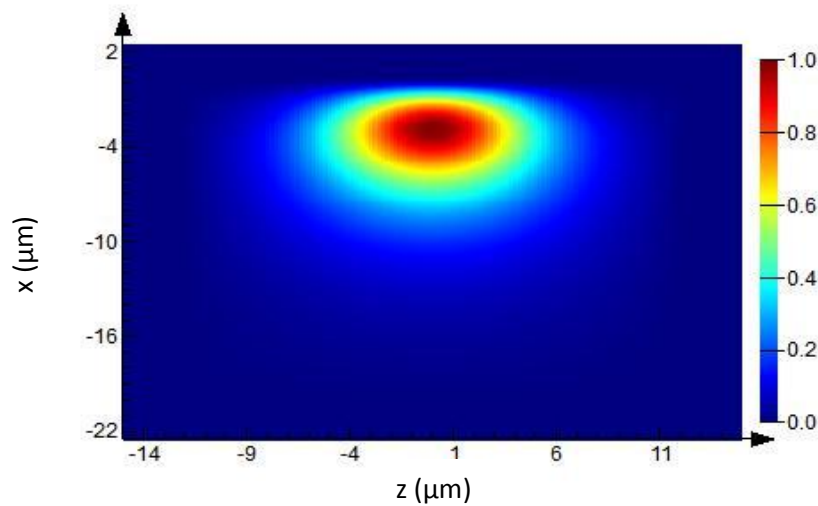


Fig. 3.10 Fundamental TM mode of Ti diffused waveguide.

ON and OFF states of the modulator were identified where the modulator shows the maximum difference between modal absorption. ON state of the modulator is when the modal absorption is the minimum and optical intensity is the maximum at the output. OFF state corresponds to the maximum modal absorption and minimum optical intensity at the output end of the waveguide. The accumulated charge carriers density corresponding to ON and OFF states for both device architectures is illustrated in Fig. 3.11.

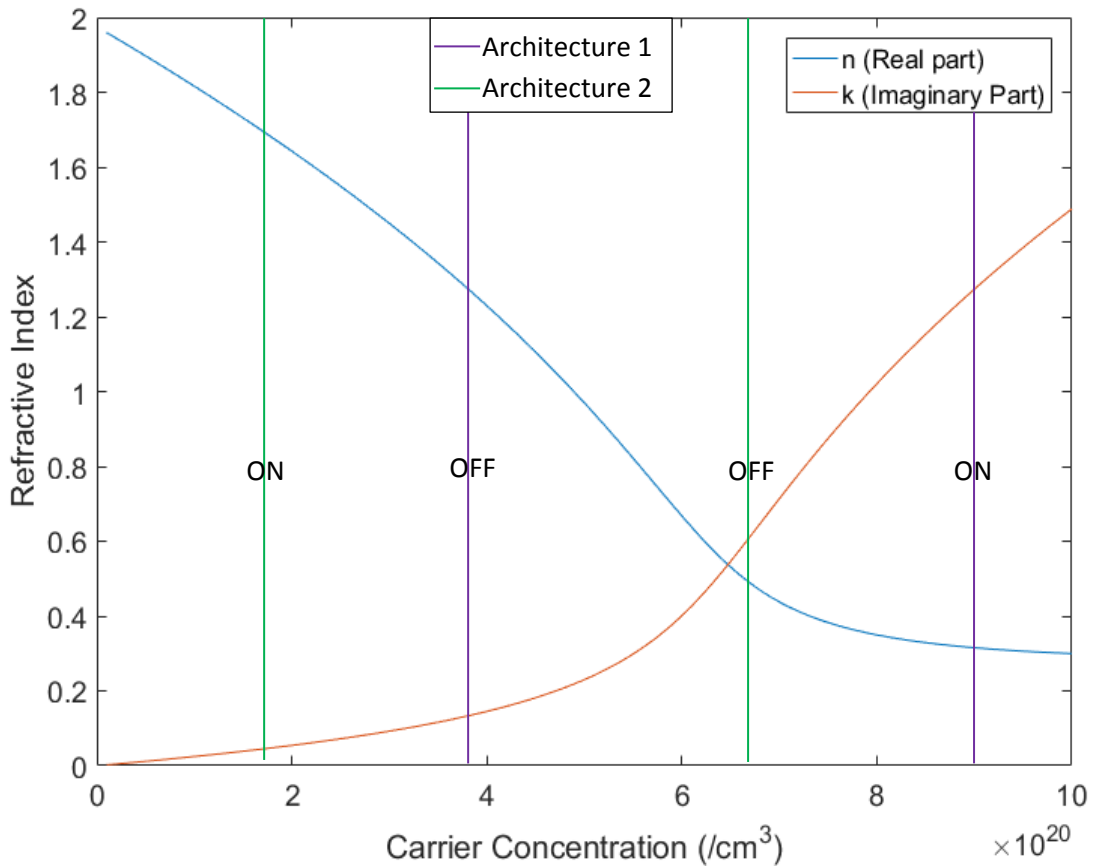
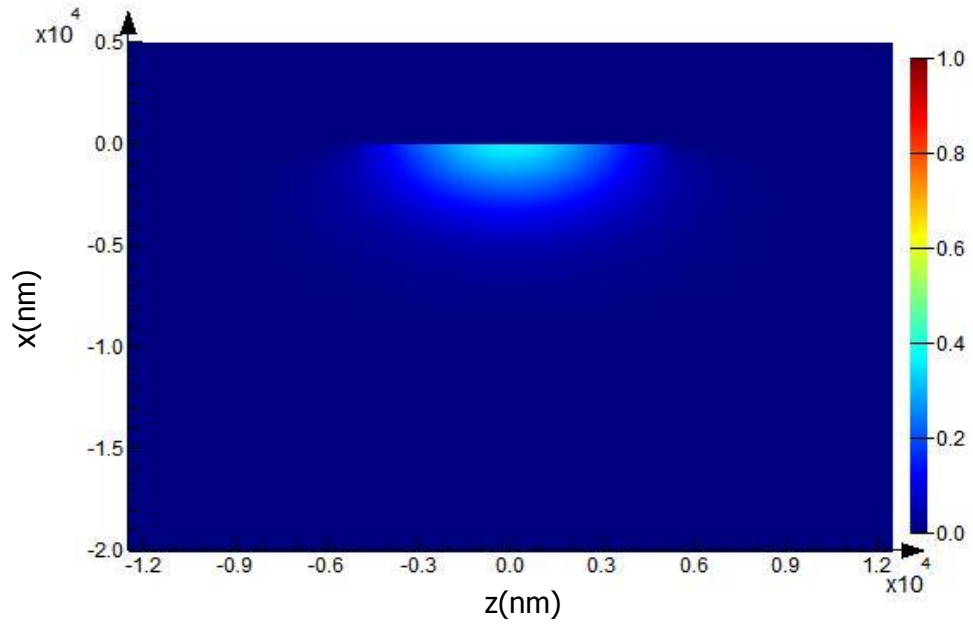


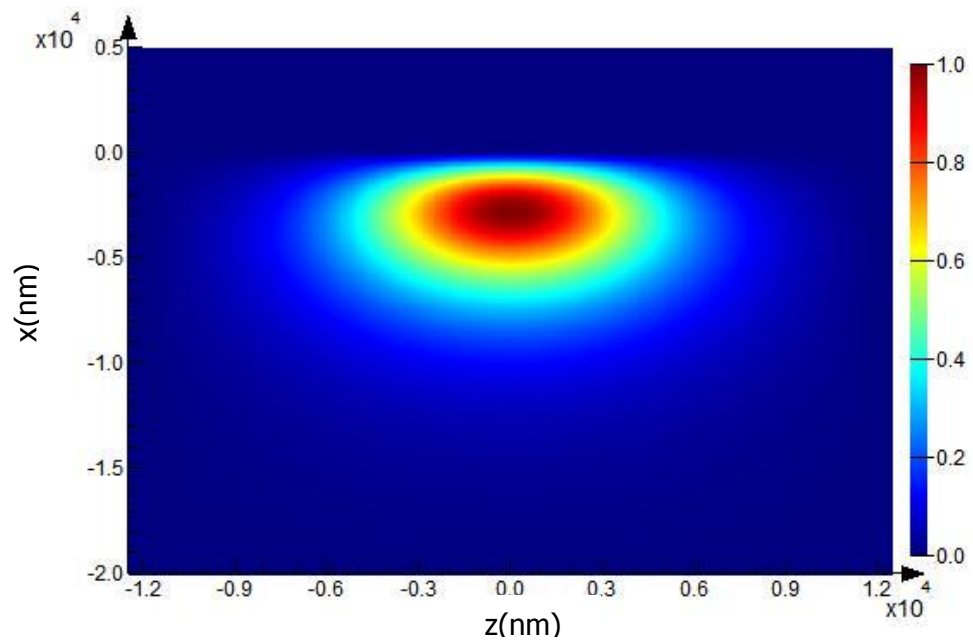
Fig. 3.11 Charge carriers concentration corresponding to the ON and the OFF states for Architecture 1 and Architecture 2.

ON state of Architecture 1 corresponds to accumulation charge density of $9.1 \times 10^{20}/\text{cm}^3$ and OFF state corresponds to charge density of $3.4 \times 10^{20}/\text{cm}^3$. The mode field distributions corresponding to ON and OFF state of the modulator structure are shown in Fig. 3.12. Eigen mode analysis shows modal absorption of $0.05\text{dB}/\mu\text{m}$ in the OFF state and the ON state practically shows zero absorption. The mode size in lithium niobate waveguide is of the order of $6\text{-}7\mu\text{m}$, limiting the interaction of the propagating mode with ITO. This leads to low extinction ratio in case of Architecture 1. Device configuration corresponding to Architecture 1 was simulated with modulator (ITO/SiO₂/Au stack) length being $100\mu\text{m}$. The extinction ratio predicted by the simulation was 5.24dB which is consistent with the Eigen mode analysis. The modulation efficiency in this configuration is low, and for 3dB modulation depth the modulator length will have to be of the order of $60\mu\text{m}$.

To overcome this deficiency, Architecture 2 was proposed which enhances the interaction of propagating mode with ITO. Eigen mode analysis of this device structure (Architecture 2) reveals that a change in carrier concentration from 1.6×10^{19} to $6.7 \times 10^{20}/\text{cm}^3$ corresponds to the maximum modulation depth. ON and OFF state field distribution profiles are shown in Fig. 3.13. OFF state occurs at epsilon near zero (ENZ) point and the mode excited is a hybrid photonic-plasmonic mode. The maximum optical field density in the OFF state occurs in ITO accumulation layer region which accounts for the high absorption of the propagating mode.

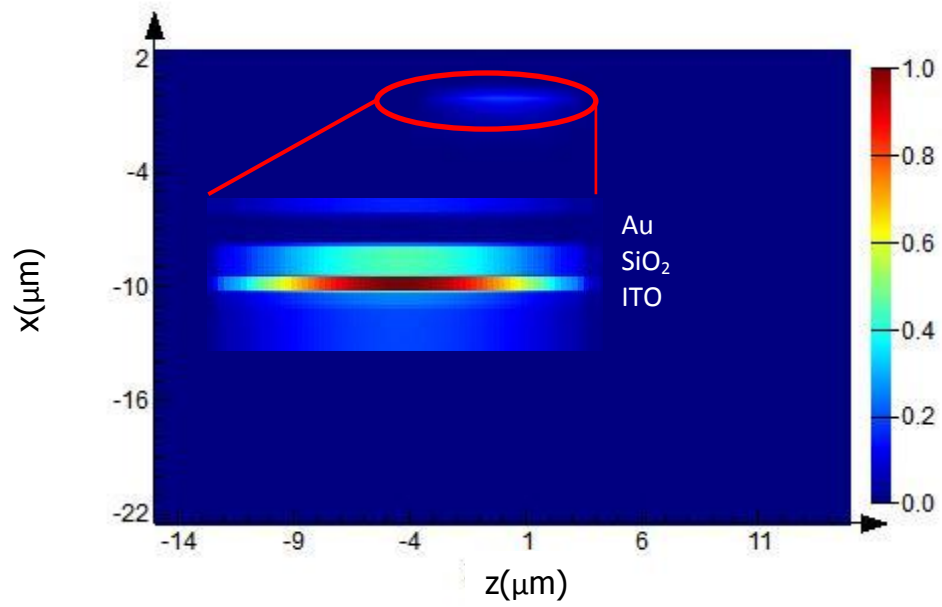


(a)

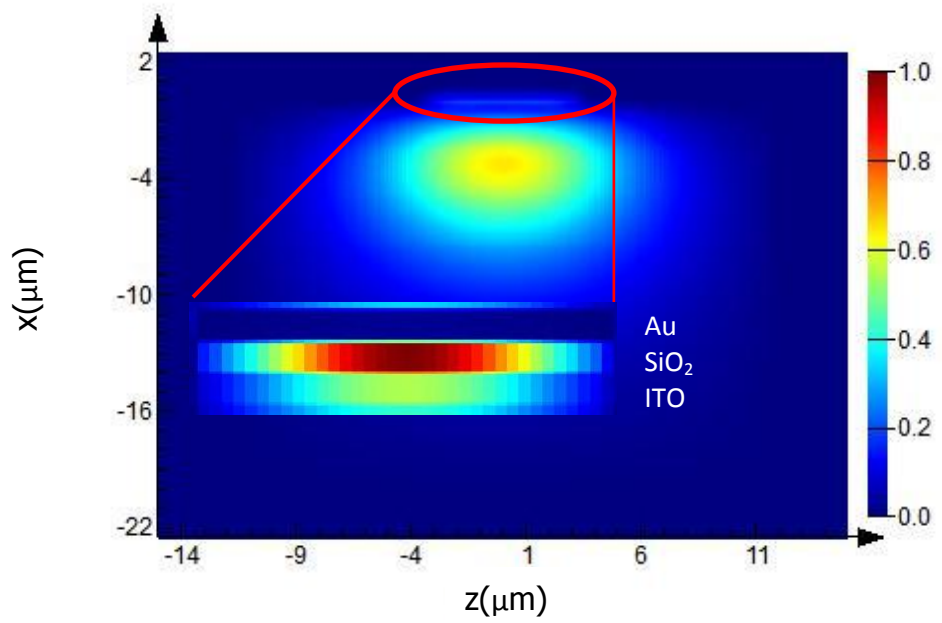


(b)

Fig. 3.12 Field profile for Modulator Architecture 1 (a) OFF state (b) ON state.



(a)



(b)

Fig. 3.13 Field profile for Modulator Architecture 2 (a) OFF state (b) ON state.

Absorption in the ON state is practically negligible because ITO acts as a lossless dielectric. In ON state maximum optical field density occurs in SiO₂ region and the optical field appears predominantly in the LN waveguide region, thus exhibiting very low propagation loss. Simulation of modulator (ITO/SiO₂/Au stack) of length 20μm was carried out and it predicted an extinction ratio of 3.75dB, which is a significant improvement over Architecture 1.

Another important performance parameter is the insertion loss of the modulator. Insertion loss primarily arises from the propagation loss in ON state of the modulator. Propagation loss is estimated to be 0.03dB and 0.04dB for Architecture 1 and Architecture 2, respectively.

Power coupling efficiency from waveguide to modulator is given by

$$\eta = \frac{4\beta_1\beta_2}{(\beta_1 + \beta_2)^2} \frac{|\int E_1^* E_2 dA|^2}{\int |E_1|^2 dA \int |E_2|^2 dA} \quad (3.17)$$

where β_1 and β_2 are propagation phase constants, E_1 and E_2 are electric field distributions in waveguide and modulator respectively and dA is the differential area element. Coupling efficiency for Architecture 1 is estimated to be approximately 99%, and 64% between hybrid waveguide and modulator for Architecture 2. The device performance of both device architectures is summarized in Table 2.

	Architecture 1 (100μm)	Architecture 2 (20μm)
Insertion loss	0.03 dB	0.04 dB
Extinction ratio	5.24 dB (0.05 dB/ μm)	3.75 dB (0.19 dB/ μm)
Coupling efficiency	99%	64%

Table 2: Performance comparison between Architecture 1 and Architecture 2.

CHAPTER IV

CONCLUSION

Photonics provides most effective means for high data rate communications. One of the major devices for communications is the modulator. Lithium niobate is used frequently for developing electro-optic modulators owing to its high electro-optic coefficients and compatibility with optical fiber. Although, the present lithium niobate modulators are very effective, they suffer from a large device footprint of the order of few millimeters.

The main objective of this thesis was to propose and investigate novel modulator architecture that can substantially reduce the device footprint. This was done following reported approaches of tunable plasmonic materials, ITO in this case. ITO owing to its high tunability of refractive index and ability to support plasmonic modes makes it a viable choice. In this investigation, ITO is used in an MOS configuration to make a modulator structure. One of the architectures proposed has stack of ITO, SiO₂ and Au over a Ti diffused waveguide. This configuration has a shortcoming because of limited interaction of the waveguide mode with ITO. To overcome this shortcoming ‘Architecture 2’ was proposed. Architecture 2 had an added TiO₂ film over the stack. TiO₂ having an overall index greater than the lithium niobate waveguide causes the mode to shift towards the surface of the waveguide and lead to increased LMI with ITO.

Mode analysis and FDTD analysis shows that Architecture 1 yields extinction ratio of $0.05\text{dB}/\mu\text{m}$ whereas Architecture 2 shows extinction ratio of $0.19\text{dB}/\mu\text{m}$. This indicates that inclusion of TiO_2 film enhances the modulator performance.

The results presented in this thesis lay the groundwork for developing plasmonic based modulators in lithium niobate. This work can be easily expanded to develop hybrid architecture consisting of tunable refractive index properties of lithium niobate and ITO to achieve better performing modulators and reduce the device footprint significantly.

REFERENCES

- [1] E.L. Wooten, K.M. Kissa, A. Yi-Yan, E.J. Murphy, D.A. Lafaw, P.F. Hallemeier, D. Maack, D.V. Attanasio, D.J. Fritz, G.J. McBrien, D.E. Bossi, "A review of lithium niobate modulators for fiber-optic communications systems," *IEEE Journal of Selected Topics in Quantum Electronics*, vol. 6, no. 1, pp. 69-82, Jan.-Feb. 2000.
- [2] V. J. Sorger, N. D. Lanzillotti-Kimura, R. M. Ma, and X. Zhang, "Ultra-compact silicon nanophotonic modulator with broadband response," *Nanophotonics*, 1, 17-22(2012).
- [3] E. Feigenbaum, K. Diest, H. A. Atwater, "Unity-order index change in transparent conducting oxides at visible frequencies," *Nano. Lett.* 10, 2111-2116 (2010).
- [4] A. P. Vasudev, J. Kang, J. Park, X. Liu & M.L. Brongersma, "Electro-optical modulation of a silicon waveguide with an "epsilon near-zero" material," *Optics Express* 21, 26387–26397 (2013).
- [5] A. Melikyan, N. Lindenmann, S. Walheim, P. M. Leufke, S. Ulrich, J. Ye, P. Vincze, H. Hahn, Th. Schimmel, C. Koos, W. Freude, and J. Leuthold, "Surface plasmon polariton absorption modulator," *Opt. Express* 19, 8855-8869 (2011).

- [6] V.E. Babicheva, A.V. Lavrinenko, "Plasmonic modulator optimized by patterning of active layer and tuning permittivity," *Opt. Commun.* 285, 5500 – 5507 (2012).
- [7] H. Nishihara, M. Haruna, T. Suhara, "Optical integrated circuits. Hiroshi Nishihara, Masamitsu Haruna, Toshiaki Suhara," New York, NY: McGraw-Hill Book Co., [1989].
- [8] María L. Calvo, Vasudevan Lakshminarayanan, "Optical waveguides: from theory to applied technologies," Boca Raton, FL: CRC Press, cop. 2007.
- [9] E. A. J. Marcatili, "Dielectric Rectangular Waveguide and Directional Coupler for Integrated Optics," *Bell System Technical Journal*, vol. 48, pp. 2071-2102, (1969).
- [10] Le N. Binh, "Guided Wave Photonics: Fundamentals and Applications with Matlab," Boca Raton, FL: CRC Press, 2012.
- [11] E. Strake, G.P. Bava, and I. Montrosset, "Guided modes of Ti:LiNbO₃ channel waveguides: A novel quasi analytical technique in comparison with scalar finite element model," *Lightwave Tech.* 6(6), p1126 (1988).
- [12] David E. Zelmon, David L. Small, and Dieter Jundt, "Infrared corrected Sellmeier coefficients for congruently grown lithium niobate and 5 mol. % magnesium oxide-doped lithium niobate," *J. Opt. Soc. Am. B* 14, 3319-3322 (1997).
- [13] W.K. Burns, "Ti diffusion in Ti: LiNbO₃ planar and channel optical waveguides," *Journal of Applied Physics.* 50, 6175-6182, Oct. 1979.

- [14] J. Kim, W.J. Sung, O. Eknayan, and C.K. Madsen, "Linear photonic frequency discriminator on As_2S_3 -ring-on-Ti:LiNbO₃ hybrid platform," *Opt. Express*, 21, pp. 24566-24573, (Oct. 2013).
- [15] J. Kischkat, S. Peters, B. Gruska, M. Semtsiv, M. Chashnikova, M. Klinkmüller, O. Fedosenko, S. Machulik, A. Aleksandrova, G. Monastyrskyi, Y. Flores, and W. T. Masselink "Mid-infrared optical properties of thin films of aluminum oxide, titanium dioxide, silicon dioxide, aluminum nitride, and silicon nitride," *Appl. Opt.* 51, 6789-6798 (2012).